https://doi.org/10.5194/egusphere-2026-5082
Preprint. Discussion started: 17 September 2026

Cloud processing signatures in boreal forest aerosol revealed by long-term in-situ observations

Liine Heikkinen[1,2], Rahul Ranjan[1,2], Sini Talvinen[1,2,3], Niels Behr[1,2,4], Sara M. Blichner[1,2], Maura Dewey[5,2,6], Lauri R. Ahonen[7], Mikael Ehn[7], Annica M. L. Ekman[5,2], Radovan Krejci[1,2], Tuukka Petäjä[7], Peter Tunved[1,2], and Ilona Riipinen[1,2]

[1]Department of Environmental Science, Stockholm University, Stockholm, Sweden
[2]Bolin Centre for Climate Research, Stockholm University, Stockholm, Sweden
[3]Department of Technical Physics, University of Eastern Finland, Kuopio, Finland
[4]Max Planck Institute for Biogeochemistry, Biogeochemical Integration, Jena, Germany
[5]Department of Meteorology, Stockholm University, Stockholm, Sweden
[6]Centre for International Climate Research (CICERO), Oslo, Norway
[7]Institute for Atmospheric and Earth System Research (INAR) /Physics, University of Helsinki, Helsinki, Finland

Correspondence: Liine Heikkinen (liine.heikkinen@aces.su.se)

Abstract

Chemical cloud processing has the potential to substantially modify atmospheric aerosol properties and influence air pollutant lifetimes, yet these processes remain challenging to empirically quantify from observations. Previous observational evidence have largely relied on short-term aircraft campaigns, providing only episodic snapshots of cloud–aerosol interactions. Here, we demonstrate that continuous ground-based observations at the SMEAR II boreal forest station enable the identification and characterization of cloud-processed aerosols over multi-year timescales. We show that bimodal aerosol number size distributions exhibiting a pronounced local minimum between the Aitken and accumulation modes –commonly referred to as the Hoppel minimum– are closely linked to the presence of clouds over the boreal forest. These bimodal distributions serve as efficient proxies for cloud-processed aerosols, allowing their physicochemical properties to be examined using long-term in-situ data. This approach provides a novel framework for studying cloud processing effects as an important, long-term complement to aircraft-based observations. Our analysis reveals that cloud processing leads to a clear enrichment of sulfate aerosol mass in the accumulation mode, while impacts on organic aerosol mass concentration and chemical composition remain insignificant. The observed impacts of cloud processing on aerosol composition are consistent with previous estimates derived from trajectory-based analyses, while extending them to a statistically robust, long-term observational context.

1. Introduction

One of the earliest recognized chemical reactions occurring in cloud droplets is the formation of sulfate, SO_4^{2-}, from sulfur dioxide, SO_2 (Calvert et al., 1985; Brandt and van Eldik, 1995), that is an oxidation reaction from sulfur in oxidation state IV (S_{IV}) to sulfur in oxidation state VI (S_{VI}). This transformation alters the physicochemical properties of cloud droplet residuals that remain in the atmosphere as aerosol particles after cloud droplet evaporation. In particular, such chemical cloud processing increases particle size and hygroscopicity (e.g., Kreidenweis et al., 2003; Petäjä et al., 2005; Crumeyrolle et al., 2008; Ervens et al., 2018), thereby enhancing their ability to scatter incoming solar radiation (Choularton et al., 1997; Zieger et al., 2013)

https://doi.org/10.5194/egusphere-2026-5082
Preprint. Discussion started: 17 September 2026

and act as cloud condensation nuclei (CCN; e.g. Petters and Kreidenweis, 2008). Although this process does not generate new CCN, it modifies existing particles such that they can activate at lower water vapor supersaturations in subsequent cloud cycles (e.g., Choularton et al., 1997). The net effect of cloud water chemistry on cloud properties can be bidirectional, potentially increasing or decreasing cloud droplet number concentrations in the following cloud cycle depending on environmental conditions (e.g., Choularton et al., 1997; Feingold and Kreidenweis, 2000; Romakkaniemi et al., 2005; Ivanova and Leighton, 2008). The sign of the cloud response mainly depends on the degree to which the addition of hygroscopic mass decreases the maximum supersaturations reached in the following cloud cycles (due to an enhanced water vapor sink) relative to the updraft velocities (sources of supersaturation) in these cloud cycles (Behr et al., 2026, in prep.).

Current estimates suggest that ~60–90% of tropospheric sulfate is formed through aqueous phase chemistry in cloud water (e.g., Ervens, 2015, and references therein), with hydrogen peroxide (H_2O_2) and ozone (O_3) acting as key oxidants. These oxidants are produced in the gas phase through photochemical reactions, linking in-cloud sulfate formation to broader atmospheric chemistry involving hydroperoxyl radical (HO_x) and nitrogen oxide (NO_x) cycles. Despite a well-established mechanistic understanding of in-cloud sulfate formation involving several oxidants, atmospheric models still struggle to reproduce observed sulfate concentrations across different environments (Bian et al., 2024; Shao et al., 2019; Turnock et al., 2015).

Attributing the mismatch in sulfate concentrations to various sulfate formation pathways (in-cloud vs photochemical gas-phase chemistry) is challenging. The difficulty partly arises from the challenge of distinguishing primary sulfate from secondary sulfate formed in the atmosphere. Additional uncertainty originates from imperfect representation of key parameters controlling in-cloud sulfate formation, such as cloud liquid water content, cloud droplet spectra and cloud water pH. While the role of these parameters on in-cloud sulfate formation is well understood, they might not be accurately modelled. Among these, cloud water pH has been identified as a particularly important and uncertain factor influencing sulfate production rates (Lee et al., 2013; see also Turnock et al., 2019).

Beyond sulfate, cloud water chemistry may also contribute to the formation of secondary organic aerosol (SOA; e.g. Ervens et al., 2011). However, SOA is traditionally understood to form via gas-phase oxidation of volatile organic compounds (VOCs) and the condensation of their oxidation products. Biogenic VOCs (BVOCs), mainly isoprene (C_5H_8) and monoterpenes ($C_{10}H_{16}$), such as α-pinene, constitute one of the main sources of non-fossil SOA (Shrivastava et al., 2017 and references therein). While the scientific understanding of SOA formation has advanced substantially in the past decades (Hallquist et al., 2009; Shrivastava et al., 2017; Bianchi et al., 2019), models still struggle to capture vertical SOA profiles (Carlton et al., 2008; Hodzic et al., 2020), and dry smog chamber experiments yield lower oxygen-to-carbon ratios (O:C) than atmospheric observations (Ervens et al., 2011), requiring long hydroxyl radical (OH) exposures (Massoli et al., 2010) in order to match the laboratory-generated SOA with ambient observations (Jimenez et al., 2009). Aqueous phase chemistry in cloud droplets could provide an alternative pathway instantly generating SOA with high characteristic O:C (e.g., Ervens et al., 2011).

https://doi.org/10.5194/egusphere-2026-5082
Preprint. Discussion started: 17 September 2026

In terms of BVOCs, more observational evidence exists in suggesting isoprene oxidation products to act as efficient aqueous-phase SOA precursors (e.g., Lim et al., 2005; Giorio et al., 2017; Lamkaddam et al., 2021) as compared to monoterpene oxidation products. While the gas-phase oxidation of monoterpenes produces several highly oxygenated reaction products that are presumed as relatively water-soluble (e.g., Kołodziejczyk et al., 2019) and reactive in the atmospheric aqueous phase, laboratory studies provide conflicting evidence regarding net impact of aqueous phase chemistry on SOA mass concentrations in monoterpene-rich environments. Some studies report substantial aqueous-phase SOA formation, for example from the photo-oxidation of *cis*-pinonic acid, a major α-pinene photo-oxidation product (Aljawhary et al., 2016). Others suggest that monoterpene-derived SOA is susceptible to photolysis and hydrolysis reactions during cloud processing, causing formation of volatile products and hence reductions in SOA concentrations (Romonosky et al., 2017).

Similar ambiguity is also found in ambient observations. Some studies report enhanced SOA mass formation associated with cloud processing (Crahan et al., 2004; Sorooshian et al., 2006, 2007), whereas others find little evidence of this process (Isokääntä et al., 2022; Wagner et al., 2015). A major reason for this ambiguity could be the scarcity of direct ambient observations of aerosol physicochemical properties in cloudy conditions. Long-term measurements are typically ground-based and often limited to fog or orographic clouds (e.g., Paglione et al., 2020; Li et al., 2020; Karlsson et al., 2021), which represent only a narrow subset of cloud types not necessarily representative of all clouds e.g. in terms of liquid water contents, droplet spectra or cloud water pH. Aircraft observations, in contrast, represent a wider range of cloud conditions, but are limited in the amounts of in-cloud data and to short-term campaigns rather than long-term observations (e.g., Hilario et al., 2021 and references therein).

Since the lifetime of aerosol particles in the troposphere can be several days, cloud-processed aerosols are continuously measured also by ground-based observations, but a major challenge in quantifying the impacts of chemical cloud processing in ambient conditions is the lack of robust observational tracers (Ervens et al., 2018). Commonly used chemical markers, such as oxalate, are not unique to in-cloud processes and can originate from multiple sources, such as biomass burning (Ervens et al., 2018; Hilario et al., 2021). Hydroxymethanesulfonate (HMS) could be a more robust marker (Munger et al., 1986; Gilardoni et al., 2016), but its quantification via commonly used aerosol measurements, such as aerosol mass spectrometry (Canagaratna et al., 2007) is challenging (Dovrou et al., 2019). Similarly, sulfur and oxygen isotopic ratios could be used to distinguish primary sulfate from in-cloud sulfate (Alexander et al., 2009; Moon et al., 2024), yet such observations are not commonly available.

In contrast, microphysical signatures of cloud processing may provide a more direct and observable indicator of in-cloud chemistry. When CCN undergo chemical cloud processing, they may (e.g., in the presence of SO_2) grow and shift size distributions toward larger particles, creating a characteristic bimodal pattern with a ”Hoppel minimum” separating an unprocessed aerosol mode from a cloud-processed aerosol mode (e.g., Hoppel et al., 1994; O’Dowd et al., 1999). This is why bimodal particle number size distributions (PNSDs) exhibiting a Hoppel minimum have been used in many studies to infer maximum supersaturation levels in

https://doi.org/10.5194/egusphere-2026-5082
Preprint. Discussion started: 17 September 2026

clouds, as the position of the Hoppel minimum could be taken to reflect the activation diameter in the clouds (Gong et al., 2023; Hoppel et al., 1996; Hudson et al., 2015).

Consistent with in-situ observations, aerosol volume size distributions retrieved from AERONET ground-based remote sensing observations also frequently exhibit bimodality following fog or low-level cloud dissipation, with a larger mode associated with cloud processed particles and a smaller mode representing the unprocessed aerosol (Eck et al., 2012). These observations across diverse environments support the interpretation of bimodality as a robust signature of chemical cloud processing. Complementary in-situ chemical analysis capturing one fog event in London also revealed aerosols rich in HMS (Dall'Osto et al., 2009) coexisting with the bimodal volume size distributions retrieved through co-located AERONET observations. Beyond this, however, bimodal PNSDs have not been exploited to investigate the associated in-cloud chemical processing. In particular, it remains unclear whether aerosol populations exhibiting Hoppel minima also show systematic differences in chemical composition.

In this study, we address the challenge in characterizing cloud-processed aerosol populations by using bimodal PNSDs with Hoppel minima as proxies for cloud processed aerosol and systematically investigate their associated chemical signatures. We focus on a boreal forest environment at the Station for Measuring Ecosystem-Atmosphere Relationships (SMEAR II) in Southern Finland, where long-term measurements of PNSDs and chemical composition are available alongside extensive meteorological and trace gas observations. At this site, aerosol mass is dominated by organic aerosol (OA) and ammonium sulfate ($(NH_4)_2SO_4$) (Heikkinen et al., 2020), with OA consisting almost completely of SOA (detected as oxygenated organic aerosol; Heikkinen et al., 2021). During the growing season, SOA forms from the oxidation of BVOCs and the subsequent condensation of their oxidation products (Mohr et al., 2019; Riipinen et al., 2012; Roldin et al., 2019). Monoterpenes are the dominant BVOCs emitted by the surrounding forest (Rantala et al., 2015), and their emissions, as well as resulting SOA formation, are strongly temperature-dependent (Guenther et al., 2012; Yli-Juuti et al., 2021). Overall, SOA concentrations at SMEAR II are highly sensitive to meteorological conditions (Petäjä et al., 2022), particularly temperature and boundary layer dynamics leading to pronounced diel cycles in SOA concentrations, especially during summer, whereas sulfate concentrations exhibit no diel cycle (Heikkinen et al., 2020, 2021).

Previous work at SMEAR II has investigated aerosol cloud processing using air mass back trajectories combined with a relative humidity (RH)-based proxy for cloud exposure (Isokääntä et al., 2022; Talvinen et al., 2025). They found that the time spent in non-precipitating clouds was associated with enhanced sulfate mass concentrations and an increased number of particles with dry diameters exceeding 200 nm, consistent with in-cloud sulfate formation. In contrast, no significant impact on OA concentrations was observed, suggesting a limited role for aqueous phase SOA formation in this environment. While the insignificant SOA response to airmass exposure to non-precipitating clouds at SMEAR II could result from a number of aqueous-phase reactions causing equal enhancements and decreases in SOA concentrations, as discussed earlier, the impact of clouds on SOA formation via gas phase chemistry perturbations via reductions in SOA precursors should not be overlooked.

https://doi.org/10.5194/egusphere-2026-5082
Preprint. Discussion started: 17 September 2026

Ambient observations can also be impacted in complex ways through the interactions between liquid water clouds and tropospheric photochemistry and oxidant concentrations (Lelieveld and Crutzen, 1990). In particular, cloud processing reduces NO_x through heterogeneous reactions involving nitrogen pentoxide (N_2O_5; Dentener and Crutzen, 1993; Heikes and Thompson, 1983; Holmes et al., 2019), while cloud attenuation of solar radiation suppresses photolysis rates can lower below-cloud NO, O_3 and HO_x concentrations (Ervens, 2015). In addition, humid and cloudy conditions may enhance ozone deposition onto wet canopy surfaces and increase stomatal uptake (Monks et al., 2015) leading to significantly reduced surface O_3 concentrations (Chen et al., 2018). Together, these processes can alter the oxidation capacity of the lower troposphere and influence SOA formation and aging, which can be further influenced by dry deposition of soluble BVOC oxidation products as well (Hodzic et al., 2014; Nguyen et al., 2015). These processes can therefore offset any SOA production that took place via cloud water chemistry. Consequently, the absence of enhanced SOA concentrations under cloud-processed conditions does not necessarily imply insignificant aqueous-phase SOA formation, but may instead reflect a near balance between competing cloud-driven processes.

Building on the work of Isokääntä et al. (2022), the present study uses bimodal PNSDs with Hoppel minima as an alternative and more physically direct proxy for cloud processing, enabling a complementary assessment of its impacts on aerosol composition and the surrounding chemical environment. The specific objectives of this study are to (i) evaluate whether bimodal PNSDs with Hoppel minima can serve as reliable indicators of cloud-processed aerosol populations, (ii) assess whether these populations exhibit systematic differences in sulfate, OA and key oxidant abundances associated with these air masses (e.g., O_3), and (iii) determine to what extent the observed differences can be attributed to chemical cloud processing as opposed to co-varying meteorological conditions. By addressing these objectives, this work provides a proof-of-concept for the use of bimodal PNSDs with Hoppel minima as proxies for cloud-processed aerosol populations, as well as a boreal forest case study to demonstrate how this proxy can be used to provide insights into chemical cloud processing in other environments in the future.

2. Methods

2.1. Data sets

The data sets used in this work are collected at the Station for Measuring Ecosystem–Atmosphere Relationships (SMEAR) II (Hari and Kulmala, 2005) in Hyytiälä, Southern Finland. SMEAR II is a boreal forest measurement site, where BVOCs are a major source of aerosol mass during the growing season (Tunved et al., 2006; Mohr et al., 2019; Roldin et al., 2019; Heikkinen et al., 2020, 2021). During the wintertime, the measured aerosol is highly influenced by anthropogenic emissions (Heikkinen et al., 2020) as well as during times when the sampled air masses have been transported over heavily industrialized areas (e.g. over St. Petersburg, Russia; Kulmala et al., 2000). Local sources of anthropogenic pollution are low, apart from the emissions from the nearby sawmill located southeast of the station (Ylivinkka et al., 2025). In the following, the measurements of key parameters at SMEAR II are described.

https://doi.org/10.5194/egusphere-2026-5082
Preprint. Discussion started: 17 September 2026

2.1.1. Particle number size distribution (PNSD)

PNSD measurements have been conducted at SMEAR II since 1996 (Mäkelä et al., 1997; Aalto et al., 2001; Dada et al., 2017) and the data set has been analyzed from multiple angles during the last decades. These data are used in this study to isolate cloud-processed aerosol populations through identifying bimodal PNSDs with Hoppel minima. The data included in this study are limited to the years 2012–2020 due to the availability of aerosol chemical composition data during this period. The measurements were conducted using a dual Differential Mobility Particle Sizer (DMPS) system (Aalto et al., 2001), which measures the PNSD from 3 to 1000 nanometers in electrical mobility diameter. The sampling is performed eight meters above ground level, providing a dried PNSD every ten minutes. These data are hereafter averaged to hourly time resolution. A more detailed description of the DMPS setup between 2012 and 2020 is provided in Heikkinen et al. (2020).

2.1.2. Aerosol chemical composition

The aerosol chemical composition measurements have been conducted using an Aerosol Chemical Speciation Monitor (ACSM; Aerodyne Research Inc., Billerica, MA, USA; Ng et al., 2011). These data are used in the study to characterize the chemical composition of cloud-processed aerosols and compare that to the composition of other types of aerosol populations. The ACSM provides the mass concentrations of OA, sulfate, nitrate, ammonium and chloride with the requirement that these chemical species need to undergo flash vaporization at 600°C, which is true for only non-refractory aerosol components. The size-range of particles measured by the ACSM is up to one micrometer in vacuum aerodynamic diameter. The sampling is conducted with a ca. 3-meter-long inlet line, which comprises a Nafion dryer after 2013. The original time resolution of the data is 30 minutes, and the data are again averaged to hourly time resolution. A more detailed description of the ACSM measurement setup and data treatment is provided in Heikkinen et al. (2020).

Further characterization from OA is also done in this work through using the oxygen-to-carbon ratios (O:C) and hydrogen-to-carbon ratios (H:C) derived from the ACSM measurements. These are based on the organic mass fractions of mass-to-change ratio (m/Q) 44 Th and m/Q 43 Th signals in the ACSM mass spectra (f_{44} and f_{43}, respectively). O:C is calculated using the formula:

$$\mathrm{O:C} = 0.079 + 4.31 \times f_{44} \quad (1)$$

and H:C using the formula

$$\mathrm{H:C} = 1.12 + 6.74 \times f_{43} - 17.77 \times f_{43}^2 \quad (2)$$

– both derived in Canagaratna et al. (2015). The applicability of ACSM in deriving O:C has received criticism due to the potential release of CO_2^+ (at m/Q 44 Th) from ACSM vaporizers (Pieber et al., 2016). As discussed in Heikkinen et al. (2021), this is a minor issue for the SMEAR II ACSM.

Finally, we use the modal chemical composition of the Aitken and accumulation modes previously derived for years 2016–2020. These data are taken from Ranjan et al. (2025). The modal composition was

https://doi.org/10.5194/egusphere-2026-5082
Preprint. Discussion started: 17 September 2026

determined by minimizing the mismatch between the measured and predicted CCN using DiffeRential Evolution Adaptive Metropolis Markov Chain Monte Carlo algorithm (DREAM-MCMC; Vrugt et al., 2013). The measured CCN concentrations were measured using a CCN counter (Droplet Measurement Technologies, Colorado, USA; e.g., Paramonov et al., 2013), while the predicted CCN concentrations were calculated from the total sub-micron aerosol composition data (ACSM data products and black carbon from Aethalometer measurements; Luoma et al., 2019) and PNSDs from DMPS (see **Sect. 2.1.1.**) using κ-Köhler theory (Petters and Kreidenweis, 2007). The DREAM-MCMC algorithm was used to explore how the mass fraction of aerosol chemical species should be distributed between the Aitken and accumulation modes to achieve the best CCN closure, while also accounting for the variability of PNSDs during each CCN measurement cycle. Sulfate detected by the ACSM are assumed to be present as ammonium sulfate ($(NH4)_2SO_4$) while nitrate is distributed between an organic nitrate and ammonium nitrate (NH_4NO_3) component. For more methodological details, we refer the reader to Ranjan et al. (2025). The modal composition is available in 2-hourly time resolution.

2.1.3. Monoterpene, sulfur dioxide and oxidant concentrations

The concentration of monoterpenes i.e., the key BVOCs emitted at SMEAR II (Rantala et al., 2015), O_3, NO, NO_2, NO_x and OH (proxy) are used in this study to evaluate how SOA precursors respond to cloudy conditions. All trace gas concentrations described in this section are averaged to hourly resolution. Monoterpene concentrations were measured using a proton transfer reaction quadrupole mass spectrometer (PTR-MS, Ionicon Analytik GmbH, Innsbruck, Austria; Lindinger and Jordan, 1998). The measurement setup is described previously in Rantala et al. (2015). Normalized sensitivities and volume mixing ratios were calculated based on the method introduced in Taipale et al. (2008). Monoterpene concentrations are taken as the signal measured at m/Q 137 Th at 8.4 meters above ground level (a.g.l.).

The measurements of NO, NO_x and ozone are also obtained from 67.2 m a.g.l. NO and NO_x were measured with an TEI 42 iTL chemiluminescence analyzer equipped with a photolytic converter (Thermo Fisher Scientific, Waltham, MA, USA) and ozone with an TEI 49C monitor (Thermo Fisher Scientific, Waltham, MA, USA). SO_2 concentrations are taken from a fluorescence TEI 43 BS (Thermo Fisher Scientific, Waltham, MA, USA) monitor from 67.2 meters a.g.l. Finally, a proxy for hydroxyl radical (OH) concentration (OH_{proxy}) is calculated through the empirical formula derived in Petäjä et al. (2009):

$$OH_{proxy} = a\mathrm{UVB}^b, \quad (3)$$

where UVB refers to the measured ultra-violet B radiation and a and b are empirical constants equating to 976.7442 and 0.1644, respectively (Kontkanen et al., 2016). UVB was measured at 18 m a.g.l. until 2017 and at 35 m a.g.l. thereafter (ensuring measurements above the forest canopy) using an SL 501A pyranometer (Solar Light, Philadelphia, PA, USA). The OH_{proxy} concentrations derived using Eq (3) are lower than those that would be modelled for SMEAR II (6.3×10^5 molec. cm^{-3} vs 17.9×10^5 molec. cm^{-3}; Petäjä et al., 2009). As suggested in Petäjä et al. (2009), the reason for the discrepancy between modeled and measured OH is likely to arise from missing VOC chemistry acting as an important sink for OH radicals.

https://doi.org/10.5194/egusphere-2026-5082
Preprint. Discussion started: 17 September 2026

2.1.4. Cloud base height and cloud fraction

Surface-based observations of cloud base height (CBH) from SMEAR II were obtained via ACTRIS Cloudnet data portal for 2012–2020. These data are used to indicate cloud presence at SMEAR II upon detection of cloud-processed aerosol populations. CBH in the data portal are provided in the CloudNet classification product (Moisseev and O'Connor, 2026) computed automatically using CloudnetPy (Tukiainen et al., 2020). This product is generated only when both cloud lidar (for liquid clouds) and radar (for ice clouds) data are available, supporting high accuracy for both cloud types. Sub-minute raw data were averaged to 1-minute resolution, after which CBH was derived for each minute. Total cloud fraction (CF, values between 0 and 1) was then calculated for each 5-minute interval from the 1-minute series as the number of cloudy minutes in each 5-minute bin divided by five. For this work, hourly averages were then calculated from the 5-minute resolution data.

2.1.5. Back trajectories and ERA5 meteorology

Airmass back trajectories were calculated using HYSPLIT (Stein et al., 2015) using ERA5 meteorology (Hersbach et al., 2020) as input. These were used as an alternative method to identify cloud-processed aerosol populations, following the method introduced in Isokääntä et al. (2022). The trajectories are calculated 96 hours backwards with hourly time resolution, and for every three hours from 2012 to 2018. The trajectory arrival height at SMEAR II was set as 100 meters. Using the relative humidity (RH) output along the trajectories, a proxy for the time the sampled air masses had spent in non-precipitating clouds during the past 24 hours is calculated as in Isokääntä et al. (2022). Thus, the time spent in non-precipitating clouds during the past 24 hours is the sum of hours in conditions where RH>94% and where ERA5 records no precipitation. Additionally, this work involves progressive precipitation filtering, in which the observations coinciding with air masses that had experienced precipitation –as reported in the HYSPLIT back trajectories– in the past 24–96 hours in 12-hour intervals were omitted from the analysis. Opposite to cloudy conditions, time the sampled air mass had been exposed to dry conditions is taken as time spent in RH<65%. This RH threshold was chosen as it was high-enough to also enable a reasonable sample size in winter, when RH is always high. The back trajectories were temporally co-located to the observations.

Airmass source region analysis was performed using HYSPLIT back trajectories to identify the impact of airmass origin on the observation frequency of bimodal PNSDs with Hoppel minima. This was done with a 1° × 1° geographic grid. The total number of PNSD observations and observations of bimodal PNSDs were calculated for each grid cell if the back trajectories indicated a minimum of 50 visits to the cell. Hereafter, the fraction of observations with bimodal PNSDs was calculated. The resulting maps identify regions where air masses are most often associated with bimodal PNSDs with Hoppel minima relative to the overall measurement periods grouped seasonally. The method for identifying the aforementioned bimodal PNSDs with Hoppel minima is described in **Section 2.2.1**.

The ERA5 meteorology along back trajectories or over SMEAR II is used in the analysis, either for calculating anomalies associated with various aerosol populations (see **Sect. 2.2.3**) or for estimating boundary

https://doi.org/10.5194/egusphere-2026-5082
Preprint. Discussion started: 17 September 2026

layer heights (BLH) at the SMEAR II station in which case we chose the BLH recorded for the station coordinates from the trajectory.

2.2. Statistical methods

2.2.1. *k*-means clustering

k-means clustering is used to classify PNSD data into *k* clusters by minimizing the squared Euclidean distance between individual observations and their respective cluster centroids. *k*-means clustering was used in this work to isolate cloud-processed aerosol populations from long-term PNSD observations (1st purpose of using *k*-means), or to determine the most common PNSD types (ideally the most cohesive cluster with most members; 2nd purpose of using *k*-means) when the HYSPLIT back trajectories indicated varying number of hours spent under non-precipitating clouds (e.g., (0,4], (4, 8] hours etc.) or under dry conditions (RH < 65%).

Prior to clustering the long-term PNSD observations to identify cloud-processed aerosol populations (1st purpose of using *k*-means), each PNSD is normalized by its integral in order to emphasize similarities in PNSD shape rather than absolute particle number concentration. The data are classified using seven clusters ($k = 7$), as this configuration performed best in identifying bimodal PNSDs exhibiting a Hoppel minimum (hereafter $PNSD_{Hoppel}$). The choice of *k* was evaluated using silhouette scores, which quantify both cluster cohesion and separation. The median silhouette score for the $PNSD_{Hoppel}$ cluster is 0.86, indicating well-defined clustering. As the aim of the *k*-means clustering is to extract a clean set of $PNSD_{Hoppel}$ profiles, additional post-clustering filtering is applied. Cluster members with silhouette scores below 0.8 are excluded, as well as members exhibiting more than one local minimum in the PNSD between 50 and 200 nm in diameter. These criteria result in the removal of approximately half of the initially identified $PNSD_{Hoppel}$ members. Finally, the remaining data are grouped into two categories: $PNSD_{Hoppel}$ and other PNSDs ($PNSD_{Other}$). Importantly, $PNSD_{Other}$ does not include the PNSDs discarded from the $PNSD_{Hoppel}$ cluster. Instead, $PNSD_{Other}$ comprises all other remaining PNSD shapes, such as distributions associated with new particle formation events or monomodal accumulation modes.

In order to identify the typical PNSD characteristics associated with different air mass transport conditions derived from HYSPLIT back trajectories (2nd purpose of using *k*-means), each *k*-means clustering is applied as an unsupervised approach. Here, *k* is determined automatically (due to the high number of conditions explored) using the elbow method. This means that *k*-means is performed for values of *k* ranging from 2 to 7, and the total sum of distances from each cluster member to every centroid of each *k*-means solution is calculated and stored. The second-order finite difference of the resulting "sum of summed distances" vector is then computed, and the optimal *k* is defined as the point where the reduction in the "sum of summed distances" vector decreases most strongly, indicating the elbow of the curve. For the selected *k*, the cluster containing the largest number of members is considered representative of the corresponding transport condition. If no single optimal *k* can be clearly identified using the elbow method, then a median PNSD is calculated instead to represent the transport condition, because it is assumed that the ideal *k* would be one.

https://doi.org/10.5194/egusphere-2026-5082
Preprint. Discussion started: 17 September 2026

2.2.2. Wilcoxon rank sum test

The Wilcoxon rank sum test is used to evaluate the statistical significance of differences in aerosol chemical composition observed in $PNSD_{Hoppel}$ vs $PNSD_{Other}$. This nonparametric, two-sided test is suitable for independent samples with different sample sizes. The null hypothesis is that the data from both samples are from continuous distributions with equal medians is rejected at $p < 0.05$ (at the 95% confidence interval).

2.2.3. Anomalies

This study makes use of anomalies calculated for periods when $PNSD_{Hoppel}$ was observed. Anomalies are defined as the difference between the median value of a given parameter (e.g., cloud fraction, CF) during each hour of the year for $PNSD_{Hoppel}$ cases and the corresponding climatological mean for that hour, calculated using all available observations (generally 2012–2020). For CF and CBH, variability in the computed anomalies is additionally characterized using interquartile ranges (IQRs). For HYSPLIT/ERA5 -based variables, RH, temperature and specific humidity anomalies along each back trajectory were calculated relative to a time- and height-resolved climatology. For every hour of the year, back time step and 200 m height bin, a climatological value was calculated by averaging the variable across all trajectories that occupied that height bin at that back time hour and were initialized at the same hour of the year. The trajectory-specific anomaly was then obtained by subtracting this climatological value from the actual variable value (e.g., RH) at the corresponding back time and height.

3. Results and discussion

We begin this section by evaluating whether bimodal PNSDs exhibiting Hoppel minima can serve as simple proxies for cloud-processed aerosol populations. We first assess the extent to which these PNSDs reflect cloud exposure in the boreal environment, and then examine the chemical composition and atmospheric conditions associated with these aerosol populations.

3.1. Bimodal PNSDs with Hoppel minima as proxies for cloud-processed aerosol

To assess whether bimodal PNSDs with Hoppel minima can be used as proxies for cloud-processed aerosol, we analyze how PNSD shape varies as a function of air mass cloud exposure history. For this purpose, we use the RH-based proxy for time spent in non-precipitating clouds (see **Sect. 2.1.5**) introduced in Isokääntä et al. (2022). The dominant PNSD shapes were identified (see **Sect. 2.2.1**) for air masses that had spent different amounts of time in non-precipitating clouds prior to arrival at SMEAR II. The analysis reveals the gradual emergence of PNSD bimodality as a function of time spent in non-precipitating clouds (**Fig. 1a**). In contrast, when the dominant PNSD shapes are examined as a function of time the airmasses had spent under dry conditions (RH<65%), the PNSD shape remains monomodal and shows little systematic evolution (**Fig. 1b**). This finding supports the interpretation of bimodal PNSDs with Hoppel minima as microphysical signatures of cloud processing.

https://doi.org/10.5194/egusphere-2026-5082
Preprint. Discussion started: 17 September 2026

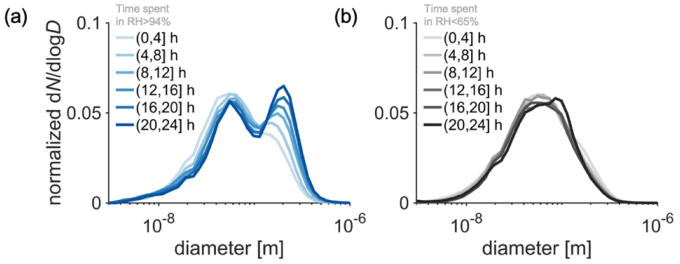

Figure 1 Evolution of PNSD shape as a function of time the sampled air mass had spent in RH>94% (a) or RH<65% (b) as predicted by the HYSPLIT back trajectories, in the absence of precipitation (see **Sect. 2.1.5**). Normalized d*N*/dlog*D* refers to the PNSD being normalized by the sum of the PNSD over all the PNSD size bins.

Next, we classified the PNSDs measured over the 8-year observation period to identify all occurrences of bimodal distributions exhibiting a Hoppel minimum ($PNSD_{Hoppel}$). Applying *k*-means clustering yields a distinct bimodal PNSD cluster, which was the most cohesive of all clusters (measured by the silhouette score, see **Sect. 2.2.1**) with a relatively stable location of the Hoppel minimum i.e., in terms of the diameter that separated the Aitken and accumulation modes (**Fig. 2a**). $PNSD_{Hoppel}$ cases occur most frequently during winter (~40% of the time) and least frequently during summer (ca. 5–10% of the time; **Fig. 2b**). Outside winter, it is more common to measure them during daytime than nighttime (**Fig. S.1**).

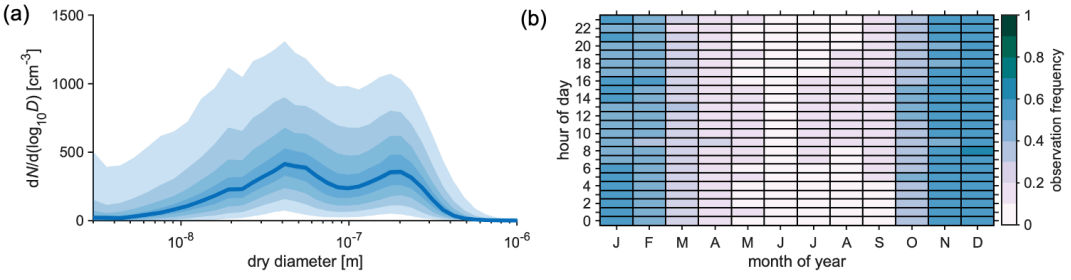

Figure 2 (a) $PNSD_{Hoppel}$ cluster. The shaded blue bands indicate the 5th–95th, 10th–90th, 15th–85th, and 25th–75th percentile ranges, from lightest to darkest, and the thick line shows the median. **(b)** The observation frequency of $PNSD_{Hoppel}$ cluster members.

Comparison of RH histories along HYSPLIT back trajectories further supports the link between $PNSD_{Hoppel}$ and cloud exposure. Consistent with **Figure 1**, airmasses associated with $PNSD_{Hoppel}$ consistently experienced higher RH than the overall climatology, particularly during spring and summer (**Fig. 3**). These positive RH anomalies are primarily driven by low temperatures rather than increased moisture (**Figs. S.2–S.3**). In winter, differences between $PNSD_{Hoppel}$ and the overall RH histories are less pronounced (**Fig. 3a**), consistent with the high occurrence frequency of $PNSD_{Hoppel}$ influencing the baseline climatology (**Fig. 2b**). However, unlike during other seasons, they coincide with increases in both temperature and specific humidity (**Figs. S.2a, S.3a**), suggesting that wintertime $PNSD_{Hoppel}$ is associated with warmer and more saturated (with respect to water vapor) air masses.

https://doi.org/10.5194/egusphere-2026-5082
Preprint. Discussion started: 17 September 2026

Because the positive spring- and summertime RH anomalies extend to short back-trajectory times (<20h; **Fig. 3b–c**), we further examine whether they can be associated with local cloud presence using ground-based observations of CF and CBH. During summer, $PNSD_{Hoppel}$ is consistently associated with enhanced CF (median 1 vs 0.78 for $PNSD_{Other}$ both at 13:00 UTC+2) and lower CBH (median 1730 m vs 2060 m with $PNSD_{Other}$ both at 13:00 UTC+2; **Fig. 4, Figs. S.4–S.5**) providing direct observational evidence that low-level clouds above SMEAR II are closely linked to the occurrence of bimodal PNSDs. In contrast, winter shows no clear CF or CBH anomalies relative to $PNSD_{Other}$, suggesting that cloud processing responsible for the bimodal PNSDs often occurred well upstream of the measurement site. We infer that recent cloud processing is required for $PNSD_{Hoppel}$ detection in summer, because rapid SOA formation (via condensation) reshapes the PNSD (e.g., Riipinen et al., 2012) and gradually obscures the cloud-processing signature over longer transport times.

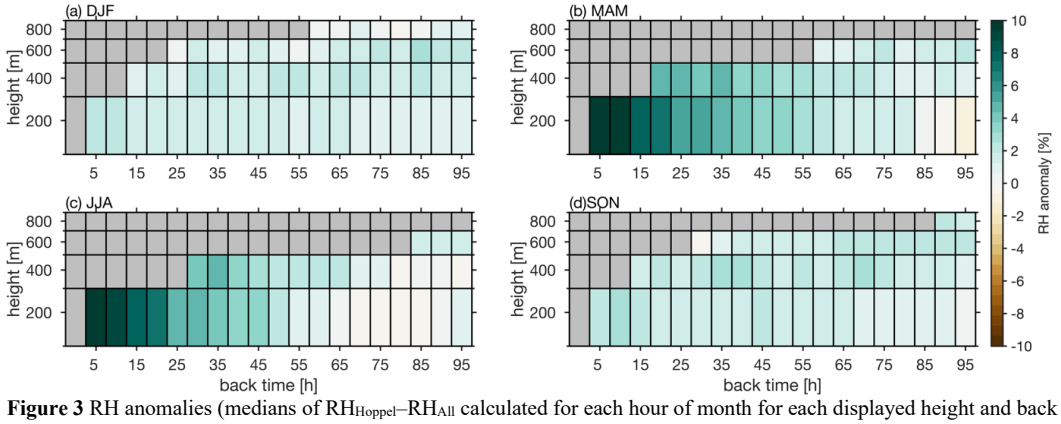

Figure 3 RH anomalies (medians of RH_{Hoppel}–RH_{All} calculated for each hour of month for each displayed height and back time cell) associated with the detection of $PNSD_{Hoppel}$ cluster members. A height-resolved 3-hourly RH climatology is derived using all HYSPLIT back trajectories run over the 8-year-long period. Different panels reflect different seasons: **(a)** winter (December–February; DJF), **(b)** spring (March–May; MAM), **(c)** summer (June–August; JJA), **(d)** fall (September–November; SON). Gray colors refer to no data.

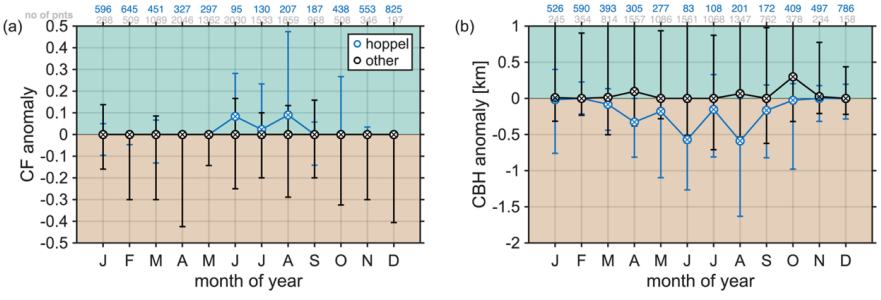

Figure 4 Median monthly cloud fraction (CF) (a) and cloud base height (CBH) (b) anomalies (e.g., medians of x_{Hoppel}–x_{All} and x_{Other}–x_{All} for each hour within a month, where x represents CF or CBH) for cases when $PNSD_{Hoppel}$ and $PNSD_{Other}$ were detected, respectively. The error bars refer to the interquartile ranges of the anomalies (see **Sect. 2.2.3** for the anomaly definition and the calculation of anomalies and anomaly IQRs). The number of data points for each month is given in gray and blue for $PNSD_{Other}$ and $PNSD_{Hoppel}$ respectively, at the top of the figures.

https://doi.org/10.5194/egusphere-2026-5082
Preprint. Discussion started: 17 September 2026

Finally, we examine the geographical origin of air masses associated with $PNSD_{Hoppel}$ using HYSPLIT back trajectories (see **Sect. 2.1.5; Fig. 5**). During winter (December to February, DJF), $PNSD_{Hoppel}$ occurs for air masses arriving from a wide range of source regions (**Fig. 5a**), consistent with long lived cloud processing signatures in background aerosol. In spring (March to May, MAM) and summer (June to August, JJA), however, a pronounced preference for northerly and northeasterly airmasses emerges (**Figs. 5b–c**). These air masses are typically cold and can provide suitable conditions for low-level cloud formation over Southern Finland, and may transport SO_2 emitted from the Kola peninsula (Riuttanen et al., 2013; Riva et al., 2019; Sipilä et al., 2021), providing precursor gases for aqueous sulfate production. As the occurrence frequency of $PNSD_{Hoppel}$ increases again in autumn (September to November, SON; **Fig. 2b**), the associated source regions become more widespread (**Fig. 5d**) as in winter. Taken together, these independent analyses consistently associate $PNSD_{Hoppel}$ with cloud processing at this boreal continental site.

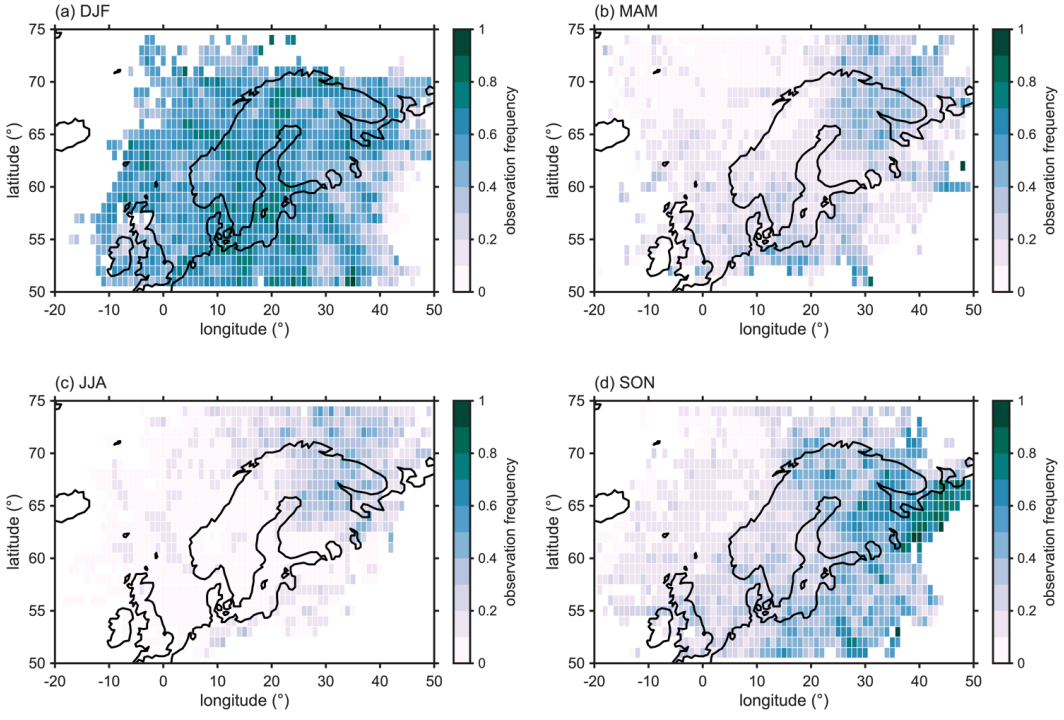

Figure 5 Observation frequency of the $PNSD_{Hoppel}$ cluster members associated with airmass origins as calculated by HYSPLIT for different seasons: **(a)** winter (December–February; DJF), **(b)** spring (March–May; MAM), **(c)** summer (June–August; JJA), **(d)** fall (September–November; SON).

3.2. Chemical characterization of cloud-processed aerosol: sulfate

Next, we examine whether the aerosol populations identified by $PNSD_{Hoppel}$ also exhibit distinct chemical characteristics. We begin by comparing sulfate mass fractions and sulfate mass concentrations between $PNSD_{Hoppel}$ and other types of PNSDs ($PNSD_{Other}$).

https://doi.org/10.5194/egusphere-2026-5082
Preprint. Discussion started: 17 September 2026

Differences between the two aerosol populations are illustrated using cumulative density function (CDF) plots (**Fig. 6**). The CDF of sulfate mass fraction for $PNSD_{Hoppel}$ is consistently shifted toward higher values relative to $PNSD_{Other}$ periods. The shift is observed across the full distribution of sulfate mass fraction values and is not driven by a small number of extreme events. Accordingly, median sulfate mass fractions are higher for $PNSD_{Hoppel}$ in all seasons: 29 vs 21% in DJF; 29 vs 18% in MAM; 17 vs 13% in JJA; 25 vs 17% in SON. In terms of absolute concentrations, median sulfate levels are also generally higher for $PNSD_{Hoppel}$, except in summer when medians are comparable (**Fig. 7**). However, these enhancements are not uniform across the sulfate mass concentration distributions: at high sulfate mass concentrations, particularly in winter and autumn, sulfate concentrations associated with $PNSD_{Other}$ can exceed those of $PNSD_{Hoppel}$.

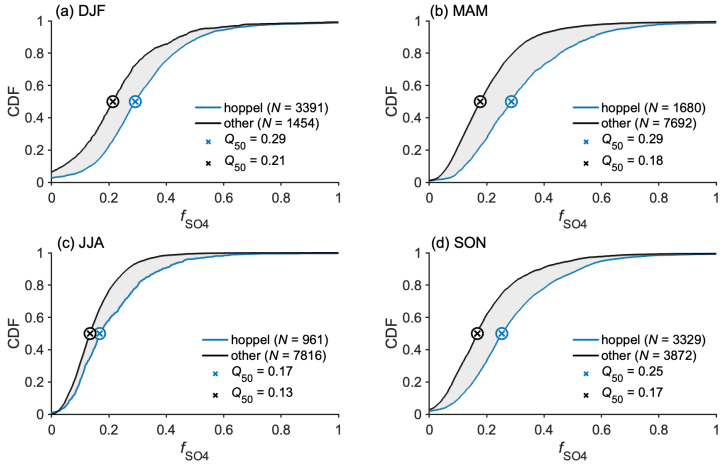

Figure 6 Cumulative density functions (CDF) of sulfate mass fractions (f_{SO4}) measured in the presence $PNSD_{Hoppel}$ (in blue) and absence (in black) of $PNSD_{Hoppel}$. The y-axes show the cumulative density function, and the x-axes show the f_{SO4}. The median values (Q_{50}, unitless) are indicated by markers and reported in the legend. Panels correspond to different seasons: **(a)** winter (December–February; DJF), **(b)** spring (March–May; MAM), **(c)** summer (June–August; JJA), **(d)** fall (September–November; SON).

https://doi.org/10.5194/egusphere-2026-5082
Preprint. Discussion started: 17 September 2026

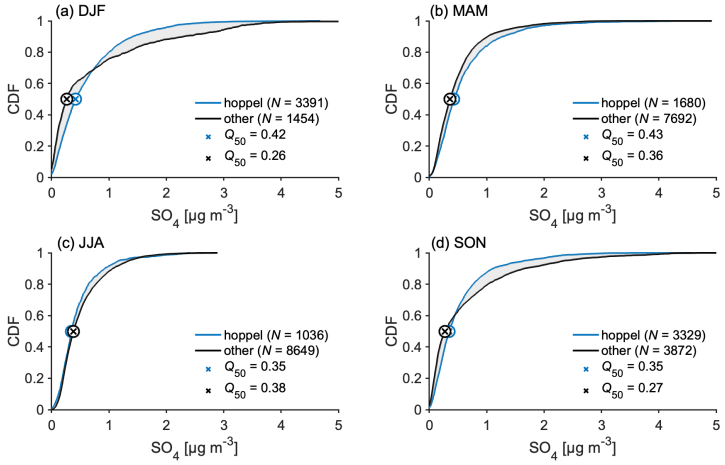

Figure 7 Cumulative density functions (CDF) of sulfate (SO_4) mass concentration measured in the presence $PNSD_{Hoppel}$ (in blue) and absence (in black) of $PNSD_{Hoppel}$. The *y*-axes show the cumulative density function, and the *x*-axes show the SO_4 mass concentrations. The median values (Q_{50}, in µg m^{-3}) are indicated by markers and reported in the legend. Panels correspond to different seasons: **(a)** winter (December–February; DJF), **(b)** spring (March–May; MAM), **(c)** summer (June–August; JJA), **(d)** fall (September–November; SON).

To examine the role of wet removal on sulfate concentrations, progressively stricter precipitation filters were applied by excluding air masses that had experienced precipitation (as estimated by ERA5) during the previous 24–96 hours. Increasing the precipitation-free period leads to systematically higher sulfate concentrations for both aerosol populations (**Fig. 8**). For $PNSD_{Hoppel}$, a weak but statistically significant increase is observed in all seasons except summer, whereas for $PNSD_{Other}$, this relationship is evident only in winter and autumn (see also **Figs S.6–S.7**). A similar picture emerges when sulfate is examined as function of accumulated precipitation (as estimated by ERA5) along the trajectories (**Fig. 9**). Under low accumulated precipitation, sulfate concentrations (and mass fractions) are consistently higher during $PNSD_{Hoppel}$, whereas sulfate decreases more rapidly with increasing precipitation than during $PNSD_{Other}$ (**Fig. 9**). This behavior most likely reflects efficient nucleation scavenging of cloud-processed aerosol, which means that the results shown both indicate that cloud processing contributes to sulfate formation, but that the observed enhancement reflects the balance between aqueous sulfate production and wet removal.

https://doi.org/10.5194/egusphere-2026-5082
Preprint. Discussion started: 17 September 2026

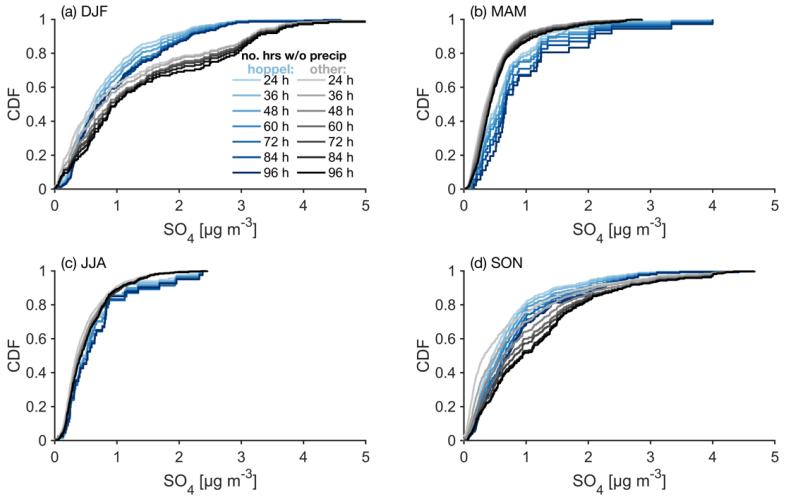

Figure 8 Cumulative density function (CDF) of sulfate (SO_4) mass concentration measured in the presence $PNSD_{Hoppel}$ (shades of blue) or absence (shades of gray) of $PNSD_{Hoppel}$. The *y*-axes show the cumulative density function, and the *x*-axes the sulfate mass concentrations. The different shades of blue and gray indicate progressively stricter precipitation filtering: trajectories that have experienced precipitation within the past 24–96 hours are increasingly excluded. The lightest shades exclude only cases with precipitation in the past 24 h, while the darkest shades exclude all cases with precipitation during the 4-day transport to the station, as calculated with HYSPLIT. Panels correspond to different seasons: **(a)** winter (December–February; DJF), **(b)** spring (March–May; MAM), **(c)** summer (June–August; JJA), **(d)** fall (September–November; SON).

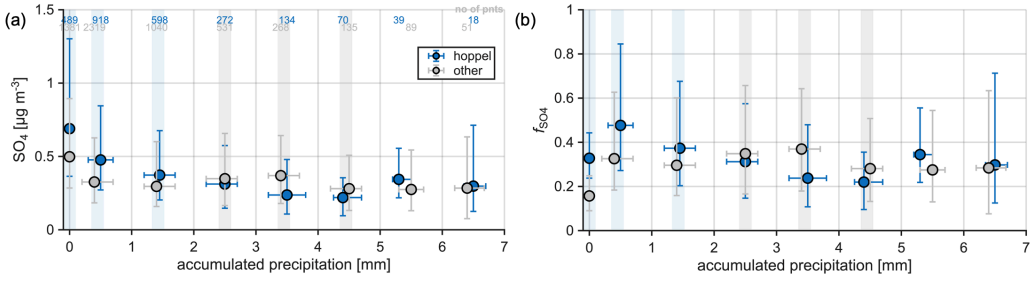

Figure 9 (**a**) Sulfate mass concentration and (**b**) sulfate mass fraction binned to accumulated precipitation as predicted by ERA5 in HYSPLIT back trajectories. The blue markers represent measurements associated with $PNSD_{Hoppel}$ while gray markers denote $PNSD_{Other}$. Numbers at the top of each panel indicate the number of data points within each OA bin for $PNSD_{Hoppel}$ (blue) and $PNSD_{Other}$ (gray) respectively. Horizontal error bars show the interquartile range (IQR) of accumulated precipitation in mm within each bin, and vertical error bars indicate the IQR of sulfate concentrations or mass fractions. Shaded regions highlight statistically significant differences between $PNSD_{Hoppel}$ and $PNSD_{Other}$, with medians of $PNSD_{Hoppel} > PNSD_{Other}$ with 95% confidence interval in blue, and $PNSD_{Hoppel} < PNSD_{Other}$ in grey.

While sulfate source-sink balance contributes to some sulfate enrichment in $PNSD_{Hoppel}$, it does not fully explain why sulfate mass fractions are significantly higher in $PNSD_{Hoppel}$ than in $PNSD_{Other}$. Instead, the elevated sulfate mass fractions are primarily driven by lower OA concentrations during $PNSD_{Hoppel}$ periods (**Fig. 10**). Because sulfate and OA dominate aerosol mass at SMEAR II (Heikkinen et al., 2020), reductions in OA lead to higher relative sulfate contributions even when absolute sulfate concentrations change only modestly. Nevertheless, when sulfate concentrations are evaluated within fixed OA ranges, $PNSD_{Hoppel}$ remains

https://doi.org/10.5194/egusphere-2026-5082
Preprint. Discussion started: 17 September 2026

consistently enriched in sulfate (**Fig. 11**). Because this feature remains, when dividing the measured ammonium sulfate into Aitken and accumulation modes (**Fig. 12; see also Figs S.9–10**), and a reverse feature is observed for SO_2 (**Fig. S.8**), we can confirm the formation of sulfate as result from chemical cloud processing. These findings highlight that bulk composition metrics, such as sulfate mass fraction, must be interpreted in the context of co-varying aerosol components. In the following section, we therefore examine the processes controlling OA concentrations associated with $PNSD_{Hoppel}$.

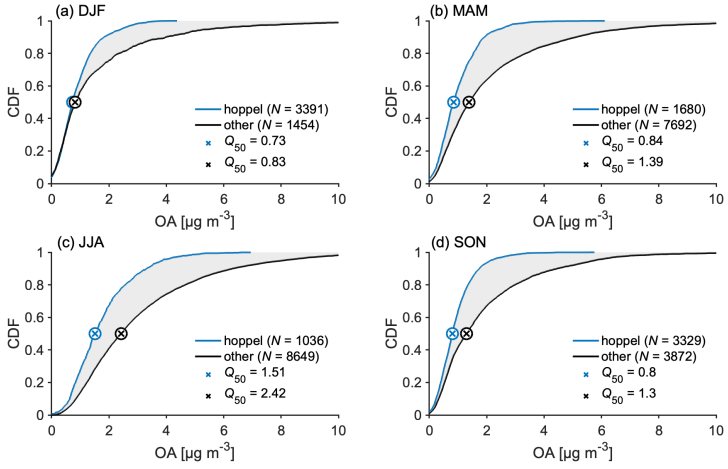

Figure 10 Cumulative density functions (CDF) of organic aerosol (OA) mass concentration measured in the presence $PNSD_{Hoppel}$ (in blue) and absence (in black) of $PNSD_{Hoppel}$. The y-axes show the cumulative density functions, and the x-axes the OA mass concentrations. The median values (Q_{50}, in µg m^{-3}) are indicated by markers and reported in the legend. Panels correspond to different seasons: **(a)** winter (December–February; DJF), **(b)** spring (March–May; MAM), **(c)** summer (June–August; JJA), **(d)** fall (September–November; SON).

https://doi.org/10.5194/egusphere-2026-5082
Preprint. Discussion started: 17 September 2026

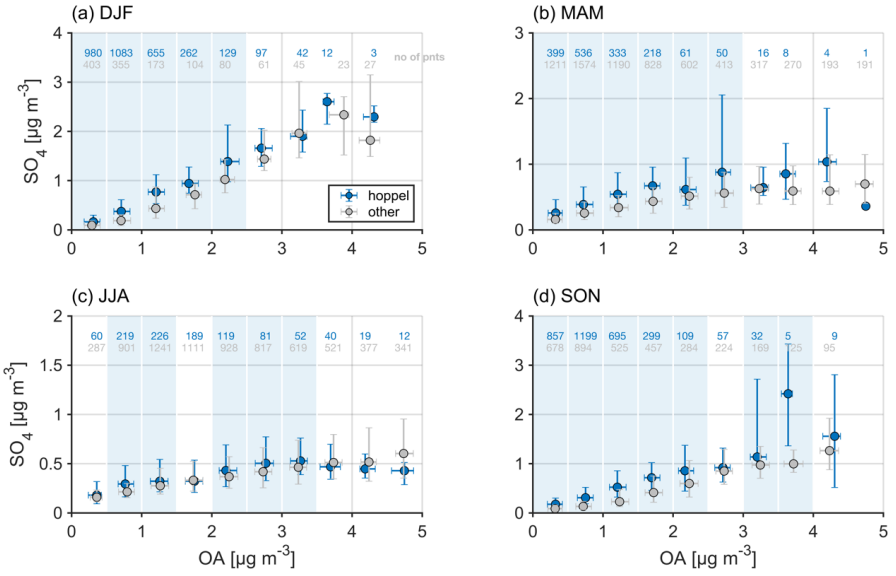

Figure 11 Median sulfate concentrations as a function of organic aerosol (OA) concentration, shown for different seasons: **(a)** winter (December–February), **(b)** spring (March–May), **(c)** summer (June–August), **(d)** fall (September–November). Blue markers represent measurements associated with $PNSD_{Hoppel}$ while gray markers denote $PNSD_{Other}$. Numbers at the top of each panel indicate the number of data points within each OA bin for $PNSD_{Hoppel}$ (blue) and $PNSD_{Other}$ (gray) respectively. Horizontal error bars show the interquartile range (IQR) of OA concentrations within each bin, and vertical error bars indicate the IQR of sulfate concentrations. Shaded regions highlight statistically significant differences between $PNSD_{Hoppel}$ and $PNSD_{Other}$ (medians of $PNSD_{Hoppel} > PNSD_{Other}$ with 95% confidence interval).

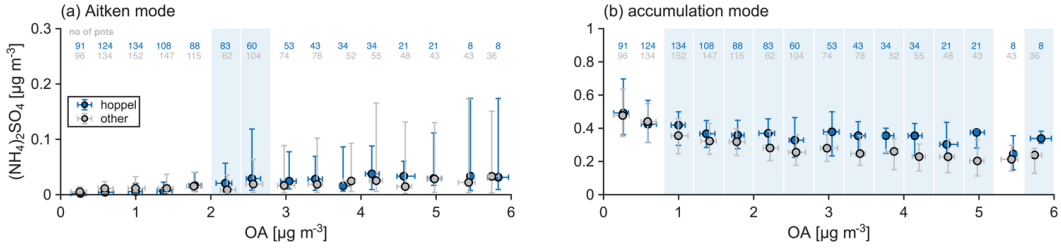

Figure 12 Median ammonium sulfate ($(NH_4)_2SO_4$) concentrations as a function of organic aerosol (OA, taken as sum of Aitken and accumulation mode OA) concentration in Aitken **(a)** and accumulation **(b)** modes, respectively. The blue markers represent measurements associated with $PNSD_{Hoppel}$ while gray markers denote $PNSD_{Other}$. Numbers at the top of each panel indicate the number of data points within each OA bin for $PNSD_{Hoppel}$ (blue) and $PNSD_{Other}$ (gray) respectively. Horizontal error bars show the interquartile range (IQR) of OA concentrations within each bin, and vertical error bars indicate the IQR of $(NH_4)_2SO_4$ concentrations. Shaded regions highlight statistically significant differences between $PNSD_{Hoppel}$ and $PNSD_{Other}$ (medians of $PNSD_{Hoppel} > PNSD_{Other}$ with 95% confidence interval).

3.3. Chemical characterization of cloud-processed aerosol: OA and oxidants

The lower OA concentrations during $PNSD_{Hoppel}$ events (**Sect. 3.2**) are primarily driven by meteorological conditions rather than chemical cloud processing. Beyond winter months, $PNSD_{Hoppel}$ periods are consistently associated with lower temperatures with median differences approximately 2°C in summer and approximately 4°C in spring and fall (**Fig. S.9**). During the growing season (T > 5 °C), emissions of BVOCs are strongly

https://doi.org/10.5194/egusphere-2026-5082
Preprint. Discussion started: 17 September 2026

temperature dependent (Guenther et al., 2012), and SOA formation at SMEAR II is largely governed by the condensation of their oxidation products (Mohr et al., 2019). As a result, OA concentrations increase exponentially with temperature (Blichner et al., 2024; Yli-Juuti et al., 2021). The colder conditions associated with $PNSD_{Hoppel}$ therefore directly translate into reduced BVOC emissions and lower SOA concentrations. This effect explains the observed OA differences during daytime, as OA concentrations for $PNSD_{Hoppel}$ and $PNSD_{Other}$ converge when compared within fixed temperature ranges (**Fig. 13a**).

At night, however, a discrepancy remains: OA concentrations are consistently higher for $PNSD_{Other}$ even under similar temperatures (**Fig. 13b**), indicating the influence of additional processes. This difference is accompanied by higher nighttime monoterpene concentrations during $PNSD_{Other}$ (**Fig. 13d**), while daytime concentrations remain comparable between the two aerosol populations (**Fig. 13c**). Because monoterpenes can be efficiently oxidized at night, for example through reactions with nitrate radicals and ozone, their higher concentrations during $PNSD_{Other}$ are consistent with enhanced nighttime SOA formation through these pathways. The nighttime monoterpene also points to differences in boundary layer dynamics: higher nighttime monoterpene concentrations under fixed temperature ranges during $PNSD_{Other}$ suggest shallower nocturnal mixing layers which trap emissions near the surface (**Fig. 13f**). The formation of these stable nighttime mixing layers may be favored during $PNSD_{Other}$ conditions because clearer skies permit greater net longwave cooling at the surface. In contrast, nocturnal low clouds during $PNSD_{Hoppel}$ periods can enhance nighttime turbulence through cloud top radiative cooling (Lilly, 1968; Hogan et al., 2009) and may reduce surface radiative cooling through downward longwave emission, thereby weakening the surface inversion and limiting the development of a shallow, stable layer. During daytime, the situation is reversed, with deeper boundary layers estimated for $PNSD_{Other}$ (**Fig. 13e**). Reduced cloud cover during $PNSD_{Other}$ allows stronger surface heating and potentially promotes deeper and more efficiently mixed boundary layers, whereas clouds associated with $PNSD_{Hoppel}$ may suppress boundary layer growth through cloud-boundary layer interactions and associated cloud mass fluxes (Van Stratum et al., 2014).

Next, we account for differences in atmospheric dilution by examining the product of OA concentration and boundary layer height, which provides an estimate of OA mass per unit surface area i.e., the OA burden. During daytime, the OA burden is significantly higher for $PNSD_{Other}$ across several temperature bins (**Fig. 13g**). At night, in contrast, OA burden is higher for $PNSD_{Hoppel}$ (**Fig. 13h**). Both day and nighttime differences reflect the corresponding differences in BLH (**Figs. 13e–f**) rather than differences in OA concentrations (**Figs. 13a–b**). However, the apparent nighttime enhancements in OA burden for $PNSD_{Hoppel}$ is not robust to seasonal separation: when a seasonal analysis is repeated e.g., for 14:00 EET (JJA) and 23:00 EET (SON), no systematic differences in nighttime or daytime OA burden remains (see **Fig. S.12**). This example demonstrates that the differences in the temperature-binned data likely reflect larger scale seasonal variability rather than effects caused by clouds. Further support for this interpretation comes from normalizing OA concentrations by monoterpene concentrations. Because both OA and monoterpene concentrations are affected by dilution, this normalization reduces the influence of boundary layer height variability. The resulting OA-to-monoterpene ratios show no clear systematic differences between $PNSD_{Hoppel}$ and $PNSD_{Other}$ during either day or night (**Figs**

https://doi.org/10.5194/egusphere-2026-5082
Preprint. Discussion started: 17 September 2026

13i–j). This suggests that, at least for the monoterpene-derived fraction of OA, cloud processing does not lead to a detectable net change in SOA formation.

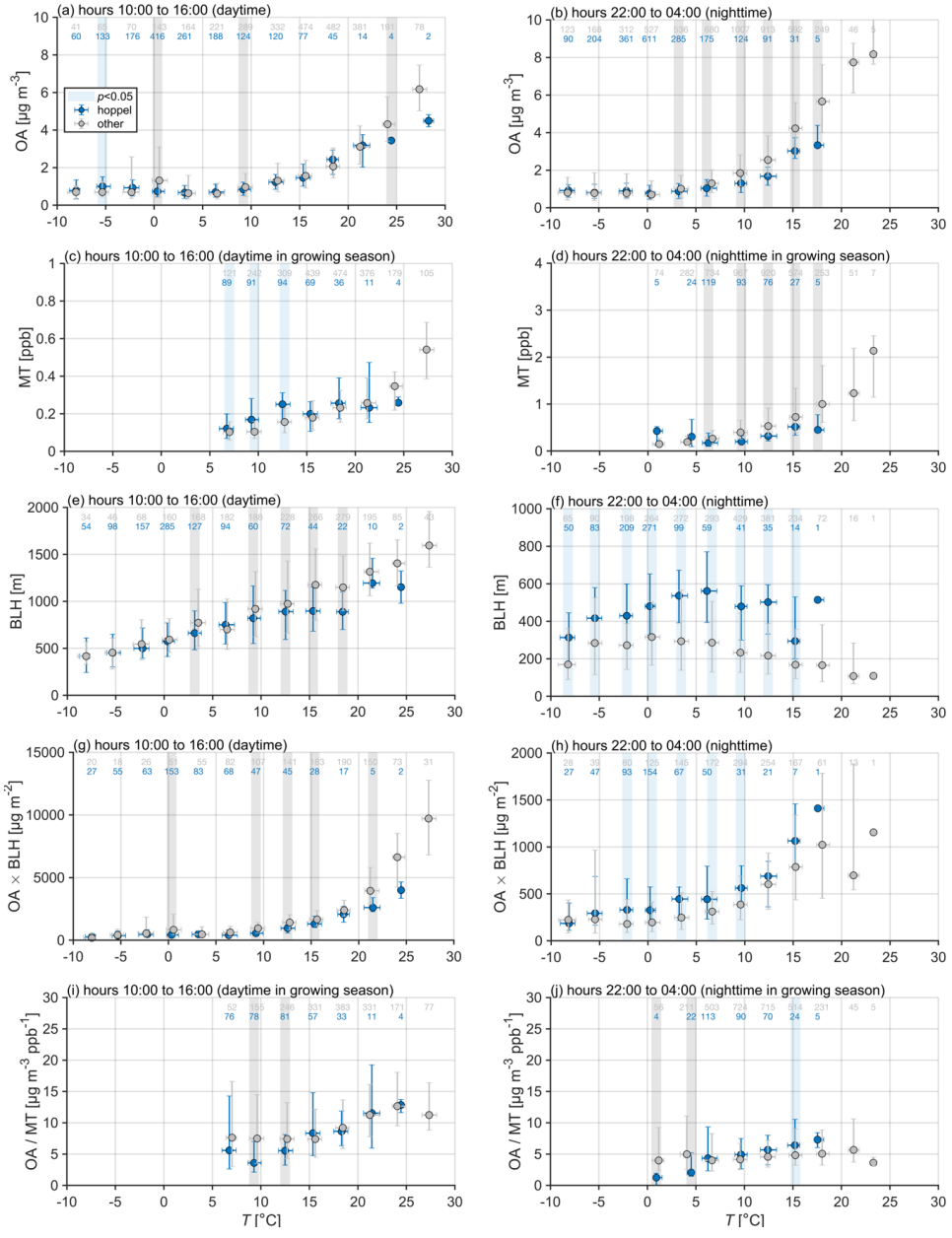

Figure 13 (a–b) Median organic aerosol (OA) concentrations, **(b–c)** median monoterpene (MT) concentrations, **(d–e)** median boundary layer heights (BLH), **(g–h)** median OA × BLH (OA burden) and **(i–j)** median OA/MT ratios as function of temperature (*T*), shown separately for daytime (10:00–16:00 EET; left panels) and nighttime (22:00–04:00 EET; right panels), respectively. Growing season is defined as time periods where daily rolling median temperature exceeds 5°C. Blue markers represent measurements associated with $PNSD_{Hoppel}$ while gray markers denote $PNSD_{Other}$. Numbers at the top of

https://doi.org/10.5194/egusphere-2026-5082
Preprint. Discussion started: 17 September 2026

each panel indicate the number of data points within each temperature bin for $PNSD_{Hoppel}$ (blue) and $PNSD_{Other}$ (gray), respectively. Horizontal error bars show the interquartile range (IQR) of temperature within each bin, and vertical errorbars indicate the IQR of the corresponding variable. Shaded regions highlight statistically significant differences (p<0.05) between $PNSD_{Hoppel}$ and $PNSD_{Other}$: Gray shadings indicate higher values for $PNSD_{Other,}$ while blue shading indicates higher values for $PNSD_{Hoppel}$.

These findings are consistent with Isokääntä et al. (2022), who also found no net enhancement of OA associated with cloud exposure during transport to SMEAR II. However, the absence of an OA increase does not necessarily imply that aqueous-phase SOA formation is negligible. In particular, cloud processing can simultaneously affect several processes controlling SOA, including aqueous-phase production, wet removal, and gas-phase oxidation. Aqueous-phase SOA formation could therefore occur without producing a detectable net enhancement in OA if it is offset by concurrent losses or by reduced gas-phase SOA production. To investigate whether cloud processing is associated with changes in the atmospheric chemical environment that could contribute to such compensation, we next compare oxidant concentrations between $PNSD_{Hoppel}$ and $PNSD_{Other}$ conditions. Specifically, we compare daytime (13:00 EET) oxidant concentrations within fixed temperature bins to minimize the influence of diel and seasonal variability.

Ozone concentrations are systematically approximately 5 ppb lower during $PNSD_{Hoppel}$ periods than during $PNSD_{Other}$ (**Fig. 14a**), corresponding to an approximately 17% reduction. This magnitude agrees well with previous estimates of cloud-induced ozone reductions summarized by Ervens (2015). Such reductions could arise either from suppressed photochemical ozone production or enhanced deposition. Because neither NO nor NO_x concentrations differ significantly between the two aerosol populations (**Figs. 14b–c**), our observations do not support reduced NO_2 photolysis as the dominant mechanism. Instead, the lower concentrations are more consistent with enhanced deposition under cloudy and humid conditions. At SMEAR II, wet canopy surfaces are known to constitute an efficient ozone sink (Chen et al., 2018; Zhou et al., 2017).

If ozone is depleted through enhanced deposition to wet surfaces, other highly soluble compounds are likely to behave similarly. Many oxygenated BVOC oxidation products possess Henry's law constants substantially larger than that of ozone and are therefore expected to be even more susceptible to removal during the aforementioned conditions. Supporting evidence is available from SMEAR II, where measurements of formic acid fluxes show persistent downward fluxes (> –1 ppb cm s^{-1}) during cloudy and humid periods (Schobesberger et al., 2016). Although formic acid is not an important SOA precursor, it represents a highly soluble BVOC oxidation product whose behavior may be indicative of other oxygenated compounds that contribute to SOA formation at SMEAR II. Model simulations accounting for the deposition of semi-volatile oxidation products predict SOA mass reductions approaching 50% over the summertime USA (Hodzic et al., 2014). Together, these observations suggest that enhanced deposition processes during certain cloudy and humid conditions may reduce the atmospheric abundance of gas-phase SOA precursors near the surface, thereby suppressing SOA formation.

Besides influencing ozone concentrations, clouds can also affect the atmospheric oxidation capacity through changes in OH concentrations. We therefore compare OH_{proxy} concentrations between $PNSD_{Hoppel}$ and $PNSD_{Other}$. During summer (T>10 °C), no significant differences are observed (**Fig. 14d**), whereas during colder

https://doi.org/10.5194/egusphere-2026-5082
Preprint. Discussion started: 17 September 2026

temperatures OH_{proxy} concentrations are on average 21% higher for $PNSD_{Other}$ than for $PNSD_{Hoppel}$. Despite these differences, both O:C nor OA concentrations (**Fig. 14e–f**) remain remarkably similar indicating comparable degrees of photochemical aging. For reference, freshly formed SOA or emitted primary organic aerosol typically exhibit lower O:C ratios (<0.5), while aqueous-phase SOA formation can yield values approaching unity (e.g., Ervens et al., 2011; Gilardoni et al., 2016). The similarity of O:C for both aerosol groups therefore does not provide evidence of reduced photochemical aging nor enhanced aqueous SOA formation for $PNSD_{Hoppel}$.

Taken together, the analyses presented here provide no evidence that cloud processing leads to a detectable net enhancement of SOA mass or O:C at SMEAR II, consistent with the findings from Isokääntä et al. (2022). However, the results also suggest that SOA formation via gas phase chemistry under cloudy conditions may be reduced, as reflected in the nearly 20% reduction in measured ozone and approximated OH concentrations. The relative importance of these competing processes cannot be quantified with the present observations.

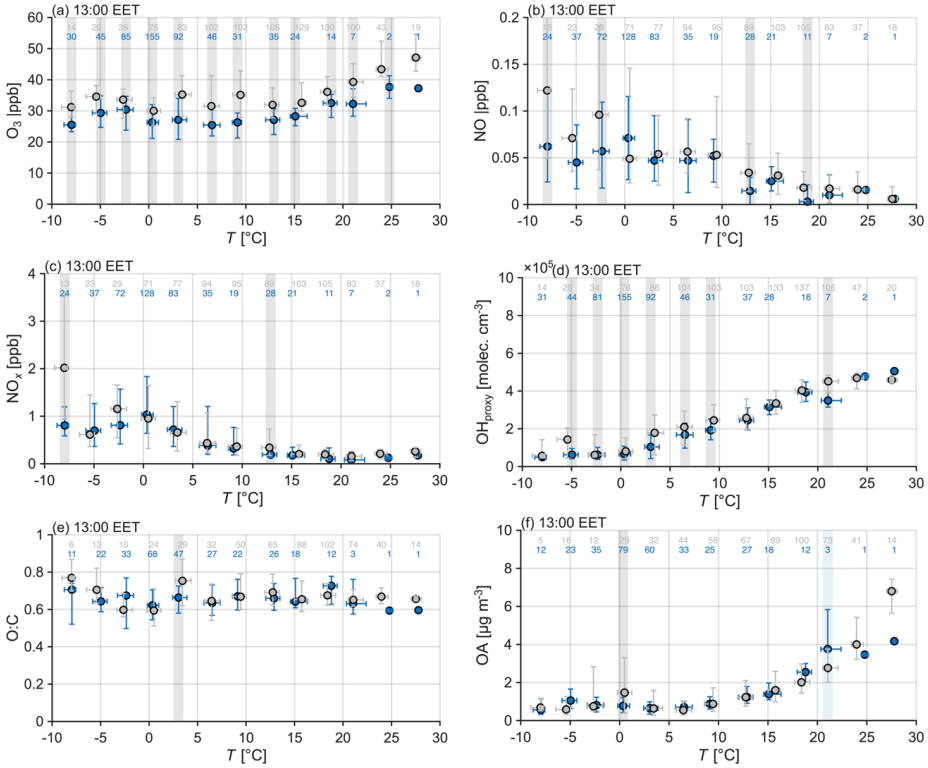

Figure 14 Median **(a)** ozone (O_3), **(b)** nitrogen monoxide (NO), **(c)** nitrogen oxides (NO_x = NO + NO_2), **(d)** hydroxyl radical (OH_{proxy}) concentrations, as well as **(e)** oxygen-to-carbon ratios (O:C) and **(f)** organic aerosol (OA) as function of temperature (*T*), shown for daytime 13:00 East European Time (EET, UTC+2). Blue markers represent measurements associated with $PNSD_{Hoppel}$ while gray markers denote other $PNSD_{Other}$. Numbers at the top of each panel indicate the number of data points within each temperature bin for $PNSD_{Hoppel}$ (blue) and $PNSD_{Other}$ (gray), respectively. Horizontal error bars show the interquartile range (IQR) of temperature within each bin, and vertical errorbars indicate the IQR of the corresponding variable. Shaded regions highlight statistically significant differences (p<0.05) between $PNSD_{Hoppel}$ and $PNSD_{Other}$: Gray shadings indicate higher values for $PNSD_{Other}$.

https://doi.org/10.5194/egusphere-2026-5082
Preprint. Discussion started: 17 September 2026

Conclusions

This study demonstrates that bimodal particle number size distributions with Hoppel minima provide a robust proxy for cloud-processed aerosol populations at SMEAR II, as their occurrence increases systematically with time spent in non-precipitating clouds and enhanced low-level cloud cover. Cloud processing leaves a clear signature in aerosol microphysics and inorganic composition, with enhanced sulfate mass fractions and a distinct enhancement of sulfate in the accumulation mode, consistent with aqueous phase sulfate production. However, the magnitude of this signal is strongly modulated by wet removal and seasonal oxidant availability, particularly during winter. Organic aerosol concentrations are typically found to be lower for bimodal aerosol size distributions with Hoppel minima than for other aerosol populations, which can primarily be explained by lower temperatures and reduced biogenic volatile organic compound emissions for the bimodal populations. Furthermore, differences in boundary layer dynamics rather than chemistry, especially at night, also contribute to lower organic aerosol concentrations. Ozone and OH_{proxy} concentrations are found to be reduced under cloudy and humid conditions, which could indicate a fine balance between reduced gas-phase SOA production and aging and aqueous-phase SOA formation. However, our results show overall that while cloud processing strongly influences inorganic aerosol composition, it does not lead to a detectable enhancement in organic aerosol concentrations in this boreal forest environment. These findings highlight the dominant role of meteorology (i.e., temperature and boundary layer height) in shaping organic aerosol variability, which should be carefully accounted for in similar studies in the future. The analysis framework should be expanded to other locations, where long-term monitoring of aerosol size distributions and chemical composition is performed with fine time resolution to gain more insights into the role of chemical cloud processing in SOA formation. In addition, model evaluations of sulfate concentrations in the presence of bimodal aerosol size distributions, with little to no precipitation history (similar to Talvinen et al., 2025), can help constrain parameterizations of aqueous phase sulfate formation in clouds.

Data availability

Modal aerosol composition: https://doi.org/10.5281/zenodo.17243685 (Dewey and Ranjan, 2025). Measurement data of PNSD, NO, NO_x, O_3, UVB and monoterpenes are available at the smartSMEAR data base (https://smear.avaa.csc.fi/; last access 19th March, 2026). Aerosol chemical composition data is available at EBAS data base (https://ebas.nilu.no/ ; last access 19th March, 2026). A compiled data file for reproducing the figures in this manuscript will be made available on the Bolin Centre for Climate Research data base (https://bolin.su.se/data ; last access 19th March, 2026).

Author contributions

Conceptualization: LH, IR, RR. Data curation: LH, TP, ME, ST, RR, MD, LRA. Formal analysis: LH. Methodology: LH, IR. Visualization: LH. Writing the original draft: LH. Review and editing the manuscript: All authors.

https://doi.org/10.5194/egusphere-2026-5082
Preprint. Discussion started: 17 September 2026

Acknowledgements

We acknowledge Pasi Aalto, Pekka Rantala, Juho Aalto and SMEAR II staff ensuring data availability and Ilona Jaakkola and Meri Räty for useful discussions.

References

Aalto, P., Hämeri, K., Becker, E., Weber, R., Salm, J., Mäkelä, J. M., Hoell, C., O'dowd, C. D., Hansson, H.-C., Väkevä, M., Koponen, I. K., Buzorius, G., and Kulmala, M.: Physical characterization of aerosol particles during nucleation events, Tellus B: Chemical and Physical Meteorology, 53, 344–358, https://doi.org/10.3402/tellusb.v53i4.17127, 2001.

Alexander, B., Park, R. J., Jacob, D. J., and Gong, S.: Transition metal-catalyzed oxidation of atmospheric sulfur: Global implications for the sulfur budget, Journal of Geophysical Research: Atmospheres, 114, https://doi.org/10.1029/2008JD010486, 2009.

Aljawhary, D., Zhao, R., Lee, A. K. Y., Wang, C., and Abbatt, J. P. D.: Kinetics, Mechanism, and Secondary Organic Aerosol Yield of Aqueous Phase Photo-oxidation of α-Pinene Oxidation Products, J. Phys. Chem. A, 120, 1395–1407, https://doi.org/10.1021/acs.jpca.5b06237, 2016.

Bian, H., Chin, M., Colarco, P. R., Apel, E. C., Blake, D. R., Froyd, K., Hornbrook, R. S., Jimenez, J., Jost, P. C., Lawler, M., Liu, M., Lund, M. T., Matsui, H., Nault, B. A., Penner, J. E., Rollins, A. W., Schill, G., Skeie, R. B., Wang, H., Xu, L., Zhang, K., and Zhu, J.: Observationally constrained analysis of sulfur cycle in the marine atmosphere with NASA ATom measurements and AeroCom model simulations, Atmospheric Chemistry and Physics, 24, 1717–1741, https://doi.org/10.5194/acp-24-1717-2024, 2024.

Bianchi, F., Kurtén, T., Riva, M., Mohr, C., Rissanen, M. P., Roldin, P., Berndt, T., Crounse, J. D., Wennberg, P. O., Mentel, T. F., Wildt, J., Junninen, H., Jokinen, T., Kulmala, M., Worsnop, D. R., Thornton, J. A., Donahue, N., Kjaergaard, H. G., and Ehn, M.: Highly Oxygenated Organic Molecules (HOM) from Gas-Phase Autoxidation Involving Peroxy Radicals: A Key Contributor to Atmospheric Aerosol, Chem. Rev., 119, 3472–3509, https://doi.org/10.1021/acs.chemrev.8b00395, 2019.

Blichner, S. M., Yli-Juuti, T., Mielonen, T., Pöhlker, C., Holopainen, E., Heikkinen, L., Mohr, C., Artaxo, P., Carbone, S., Meller, B. B., Quaresma Dias-Júnior, C., Kulmala, M., Petäjä, T., Scott, C. E., Svenhag, C., Nieradzik, L., Sporre, M., Partridge, D. G., Tovazzi, E., Virtanen, A., Kokkola, H., and Riipinen, I.: Process-evaluation of forest aerosol-cloud-climate feedback shows clear evidence from observations and large uncertainty in models, Nat Commun, 15, 969, https://doi.org/10.1038/s41467-024-45001-y, 2024.

Brandt, C. and van Eldik, R.: Transition Metal-Catalyzed Oxidation of Sulfur(IV) Oxides. Atmospheric-Relevant Processes and Mechanisms, Chem. Rev., 95, 119–190, https://doi.org/10.1021/cr00033a006, 1995.

Calvert, J. G., Lazrus, A., Kok, G. L., Heikes, B. G., Walega, J. G., Lind, J., and Cantrell, C. A.: Chemical mechanisms of acid generation in the troposphere, Nature, 317, 27–35, https://doi.org/10.1038/317027a0, 1985.

Canagaratna, M. r., Jayne, J. t., Jimenez, J. l., Allan, J. d., Alfarra, M. r., Zhang, Q., Onasch, T. b., Drewnick, F., Coe, H., Middlebrook, A., Delia, A., Williams, L. r., Trimborn, A. m., Northway, M. j., DeCarlo, P. f., Kolb, C. e., Davidovits, P., and Worsnop, D. r.: Chemical and microphysical characterization of ambient aerosols with the aerodyne aerosol mass spectrometer, Mass Spectrometry Reviews, 26, 185–222, https://doi.org/10.1002/mas.20115, 2007.

Canagaratna, M. R., Jimenez, J. L., Kroll, J. H., Chen, Q., Kessler, S. H., Massoli, P., Hildebrandt Ruiz, L., Fortner, E., Williams, L. R., Wilson, K. R., Surratt, J. D., Donahue, N. M., Jayne, J. T., and Worsnop, D. R.: Elemental ratio measurements of organic compounds using aerosol mass spectrometry: characterization, improved calibration, and implications, Atmos. Chem. Phys., 15, 253–272, https://doi.org/10.5194/acp-15-253-2015, 2015.

Carlton, A. G., Turpin, B. J., Altieri, K. E., Seitzinger, S. P., Mathur, R., Roselle, S. J., and Weber, R. J.: CMAQ Model Performance Enhanced When In-Cloud Secondary Organic Aerosol is Included: Comparisons of Organic Carbon Predictions with Measurements, Environ. Sci. Technol., 42, 8798–8802, https://doi.org/10.1021/es801192n, 2008.

https://doi.org/10.5194/egusphere-2026-5082
Preprint. Discussion started: 17 September 2026

Chen, X., Quéléver, L. L. J., Fung, P. L., Kesti, J., Rissanen, M. P., Bäck, J., Keronen, P., Junninen, H., Petäjä, T., Kerminen, V.-M., and Kulmala, M.: Observations of ozone depletion events in a Finnish boreal forest, Atmospheric Chemistry and Physics, 18, 49–63, https://doi.org/10.5194/acp-18-49-2018, 2018.

Choularton, T. W., Bower, K. N., and Gallagher, M. W.: The effect of sulphur chemistry on the scattering properties of particles, Philos Trans R Soc Lond B Biol Sci, 352, 213–220, https://doi.org/10.1098/rstb.1997.0016, 1997.

Crahan, K. K., Hegg, D., Covert, D. S., and Jonsson, H.: An exploration of aqueous oxalic acid production in the coastal marine atmosphere, Atmospheric Environment, 38, 3757–3764, https://doi.org/10.1016/j.atmosenv.2004.04.009, 2004.

Crumeyrolle, S., Gomes, L., Tulet, P., Matsuki, A., Schwarzenboeck, A., and Crahan, K.: Increase of the aerosol hygroscopicity by cloud processing in a mesoscale convective system: a case study from the AMMA campaign, Atmos. Chem. Phys., 8, 6907–6924, https://doi.org/10.5194/acp-8-6907-2008, 2008.

Dada, L., Paasonen, P., Nieminen, T., Buenrostro Mazon, S., Kontkanen, J., Peräkylä, O., Lehtipalo, K., Hussein, T., Petäjä, T., Kerminen, V.-M., Bäck, J., and Kulmala, M.: Long-term analysis of clear-sky new particle formation events and nonevents in Hyytiälä, Atmos. Chem. Phys., 17, 6227–6241, https://doi.org/10.5194/acp-17-6227-2017, 2017.

Dall'Osto, M., Harrison, R. M., Coe, H., and Williams, P.: Real-time secondary aerosol formation during a fog event in London, Atmos. Chem. Phys., 9, 2459–2469, https://doi.org/10.5194/acp-9-2459-2009, 2009.

Dentener, F. J. and Crutzen, P. J.: Reaction of N2O5 on tropospheric aerosols: Impact on the global distributions of NO x , O3, and OH, Journal of Geophysical Research: Atmospheres, 98, 7149–7163, https://doi.org/10.1029/92JD02979, 1993.

Dewey, M. and Ranjan, R.: DREAM-MCMC: Inverse-closure using DREAM-MCMC, https://doi.org/10.5281/zenodo.17243685, 2025.

Dovrou, E., Lim, C. Y., Canagaratna, M. R., Kroll, J. H., Worsnop, D. R., and Keutsch, F. N.: Measurement techniques for identifying and quantifying hydroxymethanesulfonate (HMS) in an aqueous matrix and particulate matter using aerosol mass spectrometry and ion chromatography, Atmospheric Measurement Techniques, 12, 5303–5315, https://doi.org/10.5194/amt-12-5303-2019, 2019.

Eck, T. F., Holben, B. N., Reid, J. S., Giles, D. M., Rivas, M. A., Singh, R. P., Tripathi, S. N., Bruegge, C. J., Platnick, S., Arnold, G. T., Krotkov, N. A., Carn, S. A., Sinyuk, A., Dubovik, O., Arola, A., Schafer, J. S., Artaxo, P., Smirnov, A., Chen, H., and Goloub, P.: Fog- and cloud-induced aerosol modification observed by the Aerosol Robotic Network (AERONET), Journal of Geophysical Research: Atmospheres, 117, https://doi.org/10.1029/2011JD016839, 2012.

Ervens, B.: Modeling the Processing of Aerosol and Trace Gases in Clouds and Fogs, Chem. Rev., 115, 4157–4198, https://doi.org/10.1021/cr5005887, 2015.

Ervens, B., Turpin, B. J., and Weber, R. J.: Secondary organic aerosol formation in cloud droplets and aqueous particles (aqSOA): a review of laboratory, field and model studies, Atmospheric Chemistry and Physics, 11, 11069–11102, https://doi.org/10.5194/acp-11-11069-2011, 2011.

Ervens, B., Sorooshian, A., Aldhaif, A. M., Shingler, T., Crosbie, E., Ziemba, L., Campuzano-Jost, P., Jimenez, J. L., and Wisthaler, A.: Is there an aerosol signature of chemical cloud processing?, Atmospheric Chemistry and Physics, 18, 16099–16119, https://doi.org/10.5194/acp-18-16099-2018, 2018.

Feingold, G. and Kreidenweis, S.: Does cloud processing of aerosol enhance droplet concentrations?, Journal of Geophysical Research: Atmospheres, 105, 24351–24361, https://doi.org/10.1029/2000JD900369, 2000.

Gilardoni, S., Massoli, P., Paglione, M., Giulianelli, L., Carbone, C., Rinaldi, M., Decesari, S., Sandrini, S., Costabile, F., Gobbi, G. P., Pietrogrande, M. C., Visentin, M., Scotto, F., Fuzzi, S., and Facchini, M. C.: Direct observation of aqueous secondary organic aerosol from biomass-burning emissions, Proceedings of the National Academy of Sciences, 113, 10013–10018, https://doi.org/10.1073/pnas.1602212113, 2016.

Giorio, C., Monod, A., Brégonzio-Rozier, L., DeWitt, H. L., Cazaunau, M., Temime-Roussel, B., Gratien, A., Michoud, V., Pangui, E., Ravier, S., Zielinski, A., Tapparo, A., Vermeylen, R., Claeys, M., Voisin, D., Kalberer, M., and Doussin, J.-F.: Cloud Processing of Secondary Organic Aerosol from Isoprene and Methacrolein Photooxidation, The Journal of Physical Chemistry A, 121, https://doi.org/10.1021/acs.jpca.7b05933, 2017.

https://doi.org/10.5194/egusphere-2026-5082
Preprint. Discussion started: 17 September 2026

Gong, X., Wang, Y., Xie, H., Zhang, J., Lu, Z., Wood, R., Stratmann, F., Wex, H., Liu, X., and Wang, J.: Maximum Supersaturation in the Marine Boundary Layer Clouds Over the North Atlantic, AGU Advances, 4, e2022AV000855, https://doi.org/10.1029/2022AV000855, 2023.

Guenther, A. B., Jiang, X., Heald, C. L., Sakulyanontvittaya, T., Duhl, T., Emmons, L. K., and Wang, X.: The Model of Emissions of Gases and Aerosols from Nature version 2.1 (MEGAN2.1): an extended and updated framework for modeling biogenic emissions, Geoscientific Model Development, 5, 1471–1492, https://doi.org/10.5194/gmd-5-1471-2012, 2012.

Hallquist, M., Wenger, J. C., Baltensperger, U., Rudich, Y., Simpson, D., Claeys, M., Dommen, J., Donahue, N. M., George, C., Goldstein, A. H., Hamilton, J. F., Herrmann, H., Hoffmann, T., Iinuma, Y., Jang, M., Jenkin, M. E., Jimenez, J. L., Kiendler-Scharr, A., Maenhaut, W., McFiggans, G., Mentel, T. F., Monod, A., Prévôt, A. S. H., Seinfeld, J. H., Surratt, J. D., Szmigielski, R., and Wildt, J.: The formation, properties and impact of secondary organic aerosol: current and emerging issues, Atmospheric Chemistry and Physics, 9, 5155–5236, https://doi.org/10.5194/acp-9-5155-2009, 2009.

Hari, P. and Kulmala, M.: Station for Measuring Ecosystem–Atmosphere Relations (SMEAR II), Boreal Environ. Res., 10, 8, 2005.

Heikes, B. G. and Thompson, A. M.: Effects of heterogeneous processes on NO3, HONO, and HNO3 chemistry in the troposphere, Journal of Geophysical Research: Oceans, 88, 10883–10895, https://doi.org/10.1029/JC088iC15p10883, 1983.

Heikkinen, L., Äijälä, M., Riva, M., Luoma, K., Daellenbach, K., Aalto, J., Aalto, P., Aliaga, D., Aurela, M., Keskinen, H., Makkonen, U., Rantala, P., Kulmala, M., Petäjä, T., Worsnop, D., and Ehn, M.: Long-term sub-micrometer aerosol chemical composition in the boreal forest: inter- and intra-annual variability, Atmos. Chem. Phys., 20, 3151–3180, https://doi.org/10.5194/acp-20-3151-2020, 2020.

Heikkinen, L., Äijälä, M., Daellenbach, K. R., Chen, G., Garmash, O., Aliaga, D., Graeffe, F., Räty, M., Luoma, K., Aalto, P., Kulmala, M., Petäjä, T., Worsnop, D., and Ehn, M.: Eight years of sub-micrometre organic aerosol composition data from the boreal forest characterized using a machine-learning approach, Atmos. Chem. Phys., 21, 10081–10109, https://doi.org/10.5194/acp-21-10081-2021, 2021.

Hersbach, H., Bell, B., Berrisford, P., Hirahara, S., Horányi, A., Muñoz-Sabater, J., Nicolas, J., Peubey, C., Radu, R., Schepers, D., Simmons, A., Soci, C., Abdalla, S., Abellan, X., Balsamo, G., Bechtold, P., Biavati, G., Bidlot, J., Bonavita, M., De Chiara, G., Dahlgren, P., Dee, D., Diamantakis, M., Dragani, R., Flemming, J., Forbes, R., Fuentes, M., Geer, A., Haimberger, L., Healy, S., Hogan, R. J., Hólm, E., Janisková, M., Keeley, S., Laloyaux, P., Lopez, P., Lupu, C., Radnoti, G., de Rosnay, P., Rozum, I., Vamborg, F., Villaume, S., and Thépaut, J.-N.: The ERA5 global reanalysis, Quarterly Journal of the Royal Meteorological Society, 146, 1999–2049, https://doi.org/10.1002/qj.3803, 2020.

Hilario, M. R. A., Crosbie, E., Bañaga, P. A., Betito, G., Braun, R. A., Cambaliza, M. O., Corral, A. F., Cruz, M. T., Dibb, J. E., Lorenzo, G. R., MacDonald, A. B., Robinson, C. E., Shook, M. A., Simpas, J. B., Stahl, C., Winstead, E., Ziemba, L. D., and Sorooshian, A.: Particulate Oxalate-To-Sulfate Ratio as an Aqueous Processing Marker: Similarity Across Field Campaigns and Limitations, Geophysical Research Letters, 48, e2021GL096520, https://doi.org/10.1029/2021GL096520, 2021.

Hodzic, A., Aumont, B., Knote, C., Lee-Taylor, J., Madronich, S., and Tyndall, G.: Volatility dependence of Henry's law constants of condensable organics: Application to estimate depositional loss of secondary organic aerosols, Geophysical Research Letters, 41, 4795–4804, https://doi.org/10.1002/2014GL060649, 2014.

Hodzic, A., Campuzano-Jost, P., Bian, H., Chin, M., Colarco, P. R., Day, D. A., Froyd, K. D., Heinold, B., Jo, D. S., Katich, J. M., Kodros, J. K., Nault, B. A., Pierce, J. R., Ray, E., Schacht, J., Schill, G. P., Schroder, J. C., Schwarz, J. P., Sueper, D. T., Tegen, I., Tilmes, S., Tsigaridis, K., Yu, P., and Jimenez, J. L.: Characterization of organic aerosol across the global remote troposphere: a comparison of ATom measurements and global chemistry models, Atmospheric Chemistry and Physics, 20, 4607–4635, https://doi.org/10.5194/acp-20-4607-2020, 2020.

Hogan, R. J., Grant, A. L. M., Illingworth, A. J., Pearson, G. N., and O'Connor, E. J.: Vertical velocity variance and skewness in clear and cloud-topped boundary layers as revealed by Doppler lidar, Quarterly Journal of the Royal Meteorological Society, 135, 635–643, https://doi.org/10.1002/qj.413, 2009.

https://doi.org/10.5194/egusphere-2026-5082
Preprint. Discussion started: 17 September 2026

Holmes, C. D., Bertram, T. H., Confer, K. L., Graham, K. A., Ronan, A. C., Wirks, C. K., and Shah, V.: The Role of Clouds in the Tropospheric NOx Cycle: A New Modeling Approach for Cloud Chemistry and Its Global Implications, Geophysical Research Letters, 46, 4980–4990, https://doi.org/10.1029/2019GL081990, 2019.

Hoppel, W. A., Frick, G. M., Fitzgerald, J. W., and Larson, R. E.: Marine boundary layer measurements of new particle formation and the effects nonprecipitating clouds have on aerosol size distribution, Journal of Geophysical Research: Atmospheres, 99, 14443–14459, https://doi.org/10.1029/94JD00797, 1994.

Hoppel, W. A., Frick, G. M., and Fitzgerald, J. W.: Deducing droplet concentration and supersaturation in marine boundary layer clouds from surface aerosol measurements, Journal of Geophysical Research: Atmospheres, 101, 26553–26565, https://doi.org/10.1029/96JD02243, 1996.

Hudson, J. G., Noble, S., and Tabor, S.: Cloud supersaturations from CCN spectra Hoppel minima, Journal of Geophysical Research: Atmospheres, 120, 3436–3452, https://doi.org/10.1002/2014JD022669, 2015.

Isokääntä, S., Kim, P., Mikkonen, S., Kühn, T., Kokkola, H., Yli-Juuti, T., Heikkinen, L., Luoma, K., Petäjä, T., Kipling, Z., Partridge, D., and Virtanen, A.: The effect of clouds and precipitation on the aerosol concentrations and composition in a boreal forest environment, Atmospheric Chemistry and Physics, 22, 11823–11843, https://doi.org/10.5194/acp-22-11823-2022, 2022.

Ivanova, I. T. and Leighton, H. G.: Aerosol–Cloud Interactions in a Mesoscale Model. Part II: Sensitivity to Aqueous-Phase Chemistry, Journal of the Atmospheric Sciences, 65, 309–330, https://doi.org/10.1175/2007JAS2276.1, 2008.

Jimenez, J. L., Canagaratna, M. R., Donahue, N. M., Prevot, A. S. H., Zhang, Q., Kroll, J. H., DeCarlo, P. F., Allan, J. D., Coe, H., Ng, N. L., Aiken, A. C., Docherty, K. S., Ulbrich, I. M., Grieshop, A. P., Robinson, A. L., Duplissy, J., Smith, J. D., Wilson, K. R., Lanz, V. A., Hueglin, C., Sun, Y. L., Tian, J., Laaksonen, A., Raatikainen, T., Rautiainen, J., Vaattovaara, P., Ehn, M., Kulmala, M., Tomlinson, J. M., Collins, D. R., Cubison, M. J., E., Dunlea, J., Huffman, J. A., Onasch, T. B., Alfarra, M. R., Williams, P. I., Bower, K., Kondo, Y., Schneider, J., Drewnick, F., Borrmann, S., Weimer, S., Demerjian, K., Salcedo, D., Cottrell, L., Griffin, R., Takami, A., Miyoshi, T., Hatakeyama, S., Shimono, A., Sun, J. Y., Zhang, Y. M., Dzepina, K., Kimmel, J. R., Sueper, D., Jayne, J. T., Herndon, S. C., Trimborn, A. M., Williams, L. R., Wood, E. C., Middlebrook, A. M., Kolb, C. E., Baltensperger, U., and Worsnop, D. R.: Evolution of Organic Aerosols in the Atmosphere, Science, 326, 1525–1529, https://doi.org/10.1126/science.1180353, 2009.

Karlsson, L., Krejci, R., Koike, M., Ebell, K., and Zieger, P.: A long-term study of cloud residuals from low-level Arctic clouds, Atmospheric Chemistry and Physics, 21, 8933–8959, https://doi.org/10.5194/acp-21-8933-2021, 2021.

Kołodziejczyk, A., Pyrcz, P., Pobudkowska, A., Błaziak, K., and Szmigielski, R.: Physicochemical Properties of Pinic, Pinonic, Norpinic, and Norpinonic Acids as Relevant α-Pinene Oxidation Products, J. Phys. Chem. B, 123, 8261–8267, https://doi.org/10.1021/acs.jpcb.9b05211, 2019.

Kontkanen, J., Paasonen, P., Aalto, J., Bäck, J., Rantala, P., Petäjä, T., and Kulmala, M.: Simple proxies for estimating the concentrations of monoterpenes and their oxidation products at a boreal forest site, Atmospheric Chemistry and Physics, 16, 13291–13307, https://doi.org/10.5194/acp-16-13291-2016, 2016.

Kreidenweis, S. M., Walcek, C. J., Feingold, G., Gong, W., Jacobson, M. Z., Kim, C.-H., Liu, X., Penner, J. E., Nenes, A., and Seinfeld, J. H.: Modification of aerosol mass and size distribution due to aqueous-phase SO2 oxidation in clouds: Comparisons of several models, Journal of Geophysical Research: Atmospheres, 108, https://doi.org/10.1029/2002JD002697, 2003.

Kulmala, M., Rannik, Ü., Pirjola, L., Maso, M. D., Karimäki, J., Asmi, A., Jäppinen, A., Karhu, V., Korhonen, H., Malvikko, S.-P., Puustinen, A., Raittila, J., Romakkaniemi, S., Suni, T., Yli-Koivisto, S., Paatero, J., Hari, P., and Vesala, T.: Characterization of atmospheric trace gas and aerosol concentrations at forest sites in southern and northern Finland using back trajectories, Boreal Environ. Res., 5, 22, 2000.

Lamkaddam, H., Dommen, J., Ranjithkumar, A., Gordon, H., Wehrle, G., Krechmer, J., Majluf, F., Salionov, D., Schmale, J., Bjelić, S., Carslaw, K. S., El Haddad, I., and Baltensperger, U.: Large contribution to secondary organic aerosol from isoprene cloud chemistry, Science Advances, 7, eabe2952, https://doi.org/10.1126/sciadv.abe2952, 2021.

https://doi.org/10.5194/egusphere-2026-5082
Preprint. Discussion started: 17 September 2026

Lee, L. A., Pringle, K. J., Reddington, C. L., Mann, G. W., Stier, P., Spracklen, D. V., Pierce, J. R., and Carslaw, K. S.: The magnitude and causes of uncertainty in global model simulations of cloud condensation nuclei, Atmos. Chem. Phys., 13, 8879–8914, https://doi.org/10.5194/acp-13-8879-2013, 2013.

Lelieveld, J. and Crutzen, P. J.: Influences of cloud photochemical processes on tropospheric ozone, Nature, 343, 227–233, https://doi.org/10.1038/343227a0, 1990.

Li, J., Zhu, C., Chen, H., Fu, H., Xiao, H., Wang, X., Herrmann, H., and Chen, J.: A More Important Role for the Ozone-S(IV) Oxidation Pathway Due to Decreasing Acidity in Clouds, Journal of Geophysical Research: Atmospheres, 125, e2020JD033220, https://doi.org/10.1029/2020JD033220, 2020.

Lilly, D. K.: Models of cloud-topped mixed layers under a strong inversion, Quart J Royal Meteoro Soc, 94, 292–309, https://doi.org/10.1002/qj.49709440106, 1968.

Lim, H.-J., Carlton, A. G., and Turpin, B. J.: Isoprene Forms Secondary Organic Aerosol through Cloud Processing: Model Simulations, Environ. Sci. Technol., 39, 4441–4446, https://doi.org/10.1021/es048039h, 2005.

Lindinger, W. and Jordan, A.: Proton-transfer-reaction mass spectrometry (PTR–MS): on-line monitoring of volatile organic compounds at pptv levels, Chem. Soc. Rev., 27, 347–375, https://doi.org/10.1039/A827347Z, 1998.

Luoma, K., Virkkula, A., Aalto, P., Petäjä, T., and Kulmala, M.: Over a 10-year record of aerosol optical properties at SMEAR II, Atmospheric Chemistry and Physics, 19, 11363–11382, https://doi.org/10.5194/acp-19-11363-2019, 2019.

Mäkelä, J. M., Aalto, P., Jokinen, V., Pohja, T., Nissinen, A., Palmroth, S., Markkanen, T., Seitsonen, K., Lihavainen, H., and Kulmala, M.: Observations of ultrafine aerosol particle formation and growth in boreal forest, Geophysical Research Letters, 24, 1219–1222, https://doi.org/10.1029/97GL00920, 1997.

Massoli, P., Lambe, A. T., Ahern, A. T., Williams, L. R., Ehn, M., Mikkilä, J., Canagaratna, M. R., Brune, W. H., Onasch, T. B., Jayne, J. T., Petäjä, T., Kulmala, M., Laaksonen, A., Kolb, C. E., Davidovits, P., and Worsnop, D. R.: Relationship between aerosol oxidation level and hygroscopic properties of laboratory generated secondary organic aerosol (SOA) particles, Geophysical Research Letters, 37, https://doi.org/10.1029/2010GL045258, 2010.

Mohr, C., Thornton, J. A., Heitto, A., Lopez-Hilfiker, F. D., Lutz, A., Riipinen, I., Hong, J., Donahue, N. M., Hallquist, M., Petäjä, T., Kulmala, M., and Yli-Juuti, T.: Molecular identification of organic vapors driving atmospheric nanoparticle growth, Nat Commun, 10, 4442, https://doi.org/10.1038/s41467-019-12473-2, 2019.

Moisseev, D. and O'Connor, E.: Categorize data from Hyytiälä between 1 Mar 2012 and 1 Apr 2020. ACTRIS Cloud remote sensing data centre unit (CLU). https://hdl.handle.net/21.12132/1.46881d0df9e6440b, 2026.

Monks, P. S., Archibald, A. T., Colette, A., Cooper, O., Coyle, M., Derwent, R., Fowler, D., Granier, C., Law, K. S., Mills, G. E., Stevenson, D. S., Tarasova, O., Thouret, V., Von Schneidemesser, E., Sommariva, R., Wild, O., and Williams, M. L.: Tropospheric ozone and its precursors from the urban to the global scale from air quality to short-lived climate forcer, Atmos. Chem. Phys., 15, 8889–8973, https://doi.org/10.5194/acp-15-8889-2015, 2015.

Moon, A., Jongebloed, U., Dingilian, K. K., Schauer, A. J., Chan, Y.-C., Cesler-Maloney, M., Simpson, W. R., Weber, R. J., Tsiang, L., Yazbeck, F., Zhai, S., Wedum, A., Turner, A. J., Albertin, S., Bekki, S., Savarino, J., Gribanov, K., Pratt, K. A., Costa, E. J., Anastasio, C., Sunday, M. O., Heinlein, L. M. D., Mao, J., and Alexander, B.: Primary Sulfate Is the Dominant Source of Particulate Sulfate during Winter in Fairbanks, Alaska, ACS EST Air, 1, 139–149, https://doi.org/10.1021/acsestair.3c00023, 2024.

Munger, J. W., Tiller, C., and Hoffmann, M. R.: Identification of Hydroxymethanesulfonate in Fog Water, Science, 231, 247–249, https://doi.org/10.1126/science.231.4735.247, 1986.

Ng, N. L., Herndon, S. C., Trimborn, A., Canagaratna, M. R., Croteau, P. L., Onasch, T. B., Sueper, D., Worsnop, D. R., Zhang, Q., Sun, Y. L., and Jayne, J. T.: An Aerosol Chemical Speciation Monitor (ACSM) for Routine Monitoring of the Composition and Mass Concentrations of Ambient Aerosol, Aerosol Science and Technology, 45, 780–794, https://doi.org/10.1080/02786826.2011.560211, 2011.

https://doi.org/10.5194/egusphere-2026-5082
Preprint. Discussion started: 17 September 2026

Nguyen, T. B., Crounse, J. D., Teng, A. P., St. Clair, J. M., Paulot, F., Wolfe, G. M., and Wennberg, P. O.: Rapid deposition of oxidized biogenic compounds to a temperate forest, Proceedings of the National Academy of Sciences, 112, E392–E401, https://doi.org/10.1073/pnas.1418702112, 2015.

O'Dowd, C. D., Lowe, J. A., and Smith, M. H.: Observations and modelling of aerosol growth in marine stratocumulus—case study, Atmospheric Environment, 33, 3053–3062, https://doi.org/10.1016/S1352-2310(98)00213-1, 1999.

Paglione, M., Gilardoni, S., Rinaldi, M., Decesari, S., Zanca, N., Sandrini, S., Giulianelli, L., Bacco, D., Ferrari, S., Poluzzi, V., Scotto, F., Trentini, A., Poulain, L., Herrmann, H., Wiedensohler, A., Canonaco, F., Prévôt, A. S. H., Massoli, P., Carbone, C., Facchini, M. C., and Fuzzi, S.: The impact of biomass burning and aqueous-phase processing on air quality: a multi-year source apportionment study in the Po Valley, Italy, Atmospheric Chemistry and Physics, 20, 1233–1254, https://doi.org/10.5194/acp-20-1233-2020, 2020.

Paramonov, M., Aalto, P. P., Asmi, A., Prisle, N., Kerminen, V.-M., Kulmala, M., and Petäjä, T.: The analysis of size-segregated cloud condensation nuclei counter (CCNC) data and its implications for cloud droplet activation, Atmos. Chem. Phys., 13, 10285–10301, https://doi.org/10.5194/acp-13-10285-2013, 2013.

Petäjä, T., Kerminen, V.-M., Hämeri, K., Vaattovaara, P., Joutsensaari, J., Junkermann, W., Laaksonen, A., and Kulmala, M.: Effects of SO_2 oxidation on ambient aerosol growth in water and ethanol vapours, Atmospheric Chemistry and Physics, 5, 767–779, https://doi.org/10.5194/acp-5-767-2005, 2005.

Petäjä, T., Mauldin, I. I. I., Kosciuch, E., McGrath, J., Nieminen, T., Paasonen, P., Boy, M., Adamov, A., Kotiaho, T., and Kulmala, M.: Sulfuric acid and OH concentrations in a boreal forest site, Atmospheric Chemistry and Physics, 9, 7435–7448, https://doi.org/10.5194/acp-9-7435-2009, 2009.

Petäjä, T., Tabakova, K., Manninen, A., Ezhova, E., O'Connor, E., Moisseev, D., Sinclair, V. A., Backman, J., Levula, J., Luoma, K., Virkkula, A., Paramonov, M., Räty, M., Äijälä, M., Heikkinen, L., Ehn, M., Sipilä, M., Yli-Juuti, T., Virtanen, A., Ritsche, M., Hickmon, N., Pulik, G., Rosenfeld, D., Worsnop, D. R., Bäck, J., Kulmala, M., and Kerminen, V.-M.: Influence of biogenic emissions from boreal forests on aerosol–cloud interactions, Nat. Geosci., 15, 42–47, https://doi.org/10.1038/s41561-021-00876-0, 2022.

Petters, M. D. and Kreidenweis, S. M.: A single parameter representation of hygroscopic growth and cloud condensation nucleus activity, Atmospheric Chemistry and Physics, 7, 1961–1971, https://doi.org/10.5194/acp-7-1961-2007, 2007.

Petters, M. D. and Kreidenweis, S. M.: A single parameter representation of hygroscopic growth and cloud condensation nucleus activity – Part 2: Including solubility, Atmos. Chem. Phys., 7, 2008.

Pieber, S. M., El Haddad, I., Slowik, J. G., Canagaratna, M. R., Jayne, J. T., Platt, S. M., Bozzetti, C., Daellenbach, K. R., Fröhlich, R., Vlachou, A., Klein, F., Dommen, J., Miljevic, B., Jiménez, J. L., Worsnop, D. R., Baltensperger, U., and Prévôt, A. S. H.: Inorganic Salt Interference on CO2+ in Aerodyne AMS and ACSM Organic Aerosol Composition Studies, Environ. Sci. Technol., 50, 10494–10503, https://doi.org/10.1021/acs.est.6b01035, 2016.

Ranjan, R., Dewey, M., Heikkinen, L., Ahonen, L. R., Luoma, K., Bowen, P., Petäjä, T., Ekman, A. M. L., Partridge, D. G., and Riipinen, I.: Optimizing CCN predictions through inferred modal aerosol composition – a boreal forest case study, Atmospheric Chemistry and Physics, 25, 17275–17300, https://doi.org/10.5194/acp-25-17275-2025, 2025.

Rantala, P., Aalto, J., Taipale, R., Ruuskanen, T. M., and Rinne, J.: Annual cycle of volatile organic compound exchange between a boreal pine forest and the atmosphere, Biogeosciences, 12, 5753–5770, https://doi.org/10.5194/bg-12-5753-2015, 2015.

Riipinen, I., Yli-Juuti, T., Pierce, J. R., Petäjä, T., Worsnop, D. R., Kulmala, M., and Donahue, N. M.: The contribution of organics to atmospheric nanoparticle growth, Nature Geosci, 5, 453–458, https://doi.org/10.1038/ngeo1499, 2012.

Riuttanen, L., Hulkkonen, M., Dal Maso, M., Junninen, H., and Kulmala, M.: Trajectory analysis of atmospheric transport of fine particles, SO_2 , NO_x and O_3 to the SMEAR II station in Finland in 1996–2008, Atmos. Chem. Phys., 13, 2153–2164, https://doi.org/10.5194/acp-13-2153-2013, 2013.

Riva, M., Heikkinen, L., Bell, D. M., Peräkylä, O., Zha, Q., Schallhart, S., Rissanen, M. P., Imre, D., Petäjä, T., Thornton, J. A., Zelenyuk, A., and Ehn, M.: Chemical transformations in monoterpene-derived organic aerosol enhanced by inorganic composition, npj Clim Atmos Sci, 2, 1–9, https://doi.org/10.1038/s41612-018-0058-0, 2019.

https://doi.org/10.5194/egusphere-2026-5082
Preprint. Discussion started: 17 September 2026

Roldin, P., Ehn, M., Kurtén, T., Olenius, T., Rissanen, M. P., Sarnela, N., Elm, J., Rantala, P., Hao, L., Hyttinen, N., Heikkinen, L., Worsnop, D. R., Pichelstorfer, L., Xavier, C., Clusius, P., Öström, E., Petäjä, T., Kulmala, M., Vehkamäki, H., Virtanen, A., Riipinen, I., and Boy, M.: The role of highly oxygenated organic molecules in the Boreal aerosol-cloud-climate system, Nat Commun, 10, 4370, https://doi.org/10.1038/s41467-019-12338-8, 2019.

Romakkaniemi, S., Kokkola, H., and Laaksonen, A.: Parameterization of the nitric acid effect on CCN activation, Atmospheric Chemistry and Physics, 5, 879–885, https://doi.org/10.5194/acp-5-879-2005, 2005.

Romonosky, D. E., Li, Y., Shiraiwa, M., Laskin, A., Laskin, J., and Nizkorodov, S. A.: Aqueous Photochemistry of Secondary Organic Aerosol of α-Pinene and α-Humulene Oxidized with Ozone, Hydroxyl Radical, and Nitrate Radical, J. Phys. Chem. A, 121, 1298–1309, https://doi.org/10.1021/acs.jpca.6b10900, 2017.

Schobesberger, S., Lopez-Hilfiker, F. D., Taipale, D., Millet, D. B., D'Ambro, E. L., Rantala, P., Mammarella, I., Zhou, P., Wolfe, G. M., Lee, B. H., Boy, M., and Thornton, J. A.: High upward fluxes of formic acid from a boreal forest canopy, Geophysical Research Letters, 43, 9342–9351, https://doi.org/10.1002/2016GL069599, 2016.

Shao, J., Chen, Q., Wang, Y., Lu, X., He, P., Sun, Y., Shah, V., Martin, R. V., Philip, S., Song, S., Zhao, Y., Xie, Z., Zhang, L., and Alexander, B.: Heterogeneous sulfate aerosol formation mechanisms during wintertime Chinese haze events: air quality model assessment using observations of sulfate oxygen isotopes in Beijing, Atmospheric Chemistry and Physics, 19, 6107–6123, https://doi.org/10.5194/acp-19-6107-2019, 2019.

Shrivastava, M., Cappa, C. D., Fan, J., Goldstein, A. H., Guenther, A. B., Jimenez, J. L., Kuang, C., Laskin, A., Martin, S. T., Ng, N. L., Petaja, T., Pierce, J. R., Rasch, P. J., Roldin, P., Seinfeld, J. H., Shilling, J., Smith, J. N., Thornton, J. A., Volkamer, R., Wang, J., Worsnop, D. R., Zaveri, R. A., Zelenyuk, A., and Zhang, Q.: Recent advances in understanding secondary organic aerosol: Implications for global climate forcing, Reviews of Geophysics, 55, 509–559, https://doi.org/10.1002/2016RG000540, 2017.

Sipilä, M., Sarnela, N., Neitola, K., Laitinen, T., Kemppainen, D., Beck, L., Duplissy, E.-M., Kuittinen, S., Lehmusjärvi, T., Lampilahti, J., Kerminen, V.-M., Lehtipalo, K., Aalto, P. P., Keronen, P., Siivola, E., Rantala, P. A., Worsnop, D. R., Kulmala, M., Jokinen, T., and Petäjä, T.: Wintertime subarctic new particle formation from Kola Peninsula sulfur emissions, Atmospheric Chemistry and Physics, 21, 17559–17576, https://doi.org/10.5194/acp-21-17559-2021, 2021.

Sorooshian, A., Varutbangkul, V., Brechtel, F. J., Ervens, B., Feingold, G., Bahreini, R., Murphy, S. M., Holloway, J. S., Atlas, E. L., Buzorius, G., Jonsson, H., Flagan, R. C., and Seinfeld, J. H.: Oxalic acid in clear and cloudy atmospheres: Analysis of data from International Consortium for Atmospheric Research on Transport and Transformation 2004, Journal of Geophysical Research: Atmospheres, 111, https://doi.org/10.1029/2005JD006880, 2006.

Sorooshian, A., Lu, M.-L., Brechtel, F. J., Jonsson, H., Feingold, G., Flagan, R. C., and Seinfeld, J. H.: On the Source of Organic Acid Aerosol Layers above Clouds, Environ. Sci. Technol., 41, 4647–4654, https://doi.org/10.1021/es0630442, 2007.

Stein, A. F., Draxler, R. R., Rolph, G. D., Stunder, B. J. B., Cohen, M. D., and Ngan, F.: NOAA's HYSPLIT Atmospheric Transport and Dispersion Modeling System, Bulletin of the American Meteorological Society, 96, 2059–2077, https://doi.org/10.1175/BAMS-D-14-00110.1, 2015.

Taipale, R., Ruuskanen, T. M., Rinne, J., Kajos, M. K., Hakola, H., Pohja, T., and Kulmala, M.: Technical Note: Quantitative long-term measurements of VOC concentrations by PTR-MS – measurement, calibration, and volume mixing ratio calculation methods, Atmospheric Chemistry and Physics, 8, 6681–6698, https://doi.org/10.5194/acp-8-6681-2008, 2008.

Talvinen, S., Kim, P., Tovazzi, E., Holopainen, E., Cremer, R., Kühn, T., Kokkola, H., Kipling, Z., Neubauer, D., Teixeira, J. C., Sellar, A., Watson-Parris, D., Yang, Y., Zhu, J., Krishnan, S., Virtanen, A., and Partridge, D. G.: Towards an improved understanding of the impact of clouds and precipitation on the representation of aerosols over the Boreal Forest in GCMs, https://doi.org/10.5194/egusphere-2025-721, 21 March 2025., 2025.

Tukiainen, S., O'Connor, E., and Korpinen, A.: CloudnetPy: A Python package for processing cloud remote sensing data, Journal of Open Source Software, 5, 2123, https://doi.org/10.21105/joss.02123, 2020.

https://doi.org/10.5194/egusphere-2026-5082
Preprint. Discussion started: 17 September 2026

Tunved, P., Hansson, H.-C., Kerminen, V.-M., Ström, J., Maso, M. D., Lihavainen, H., Viisanen, Y., Aalto, P. P., Komppula, M., and Kulmala, M.: High Natural Aerosol Loading over Boreal Forests, Science, 312, 261–263, https://doi.org/10.1126/science.1123052, 2006.

Turnock, S. T., Spracklen, D. V., Carslaw, K. S., Mann, G. W., Woodhouse, M. T., Forster, P. M., Haywood, J., Johnson, C. E., Dalvi, M., Bellouin, N., and Sanchez-Lorenzo, A.: Modelled and observed changes in aerosols and surface solar radiation over Europe between 1960 and 2009, Atmos. Chem. Phys., 15, 9477–9500, https://doi.org/10.5194/acp-15-9477-2015, 2015.

Turnock, S. T., Mann, G. W., Woodhouse, M. T., Dalvi, M., O'Connor, F. M., Carslaw, K. S., and Spracklen, D. V.: The Impact of Changes in Cloud Water pH on Aerosol Radiative Forcing, Geophysical Research Letters, 46, 4039–4048, https://doi.org/10.1029/2019GL082067, 2019.

Van Stratum, B. J. H., Arellano, J. V.-G. de, Heerwaarden, C. C. van, and Ouwersloot, H. G.: Subcloud-Layer Feedbacks Driven by the Mass Flux of Shallow Cumulus Convection over Land, Journal of the Atmospheric Sciences, 71, 881–895, https://doi.org/10.1175/JAS-D-13-0192.1, 2014.

Vrugt, J. A., Ter Braak, C. J. F., Diks, C. G. H., and Schoups, G.: Hydrologic data assimilation using particle Markov chain Monte Carlo simulation: Theory, concepts and applications, Advances in Water Resources, 51, 457–478, https://doi.org/10.1016/j.advwatres.2012.04.002, 2013.

Wagner, N. L., Brock, C. A., Angevine, W. M., Beyersdorf, A., Campuzano-Jost, P., Day, D., de Gouw, J. A., Diskin, G. S., Gordon, T. D., Graus, M. G., Holloway, J. S., Huey, G., Jimenez, J. L., Lack, D. A., Liao, J., Liu, X., Markovic, M. Z., Middlebrook, A. M., Mikoviny, T., Peischl, J., Perring, A. E., Richardson, M. S., Ryerson, T. B., Schwarz, J. P., Warneke, C., Welti, A., Wisthaler, A., Ziemba, L. D., and Murphy, D. M.: In situ vertical profiles of aerosol extinction, mass, and composition over the southeast United States during SENEX and SEAC^{4}RS: observations of a modest aerosol enhancement aloft, Atmospheric Chemistry and Physics, 15, 7085–7102, https://doi.org/10.5194/acp-15-7085-2015, 2015.

Yli-Juuti, T., Mielonen, T., Heikkinen, L., Arola, A., Ehn, M., Isokääntä, S., Keskinen, H.-M., Kulmala, M., Laakso, A., Lipponen, A., Luoma, K., Mikkonen, S., Nieminen, T., Paasonen, P., Petäjä, T., Romakkaniemi, S., Tonttila, J., Kokkola, H., and Virtanen, A.: Significance of the organic aerosol driven climate feedback in the boreal area, Nat Commun, 12, 5637, https://doi.org/10.1038/s41467-021-25850-7, 2021.

Ylivinkka, I., Di Natale, C., Mikkelsen, M. K., Nissinen, A., Pennacchio, L., Strömberg, J., Saranko, O., Utriainen, L., Valiati, R., Aalto, J., Banerji, S., Heikkinen, L., Lintunen, A., Luoma, K., Peräkylä, O., Sarnela, N., Taipale, D., Taipale, R., Thomas, S. J., Zhang, X., and Kulmala, M.: Intervention of pollution episodes from nearby sawmills to ecosystem-atmosphere interactions studied in a boreal forest at SMEAR II, https://doi.org/10.60910/BER2025.727E-SW95, 2025.

Zhou, P., Ganzeveld, L., Rannik, Ü., Zhou, L., Gierens, R., Taipale, D., Mammarella, I., and Boy, M.: Simulating ozone dry deposition at a boreal forest with a multi-layer canopy deposition model, Atmos. Chem. Phys., 17, 1361–1379, https://doi.org/10.5194/acp-17-1361-2017, 2017.

Zieger, P., Fierz-Schmidhauser, R., Weingartner, E., and Baltensperger, U.: Effects of relative humidity on aerosol light scattering: results from different European sites, Atmospheric Chemistry and Physics, 13, 10609–10631, https://doi.org/10.5194/acp-13-10609-2013, 2013.